Contents lists available at ScienceDirect

# Cancer Letters

# Hepatocellular carcinoma with progenitor cell features distinguishable by the hepatic stem/progenitor cell marker NCAM

Atsunori Tsuchiya *, Hiroteru Kamimura, Yasushi Tamura, Masaaki Takamura, Satoshi Yamagiwa, Takeshi Suda, Minoru Nomoto, Yutaka Aoyagi

Division of Gastroenterology and Hepatology, Graduate School of Medical and Dental Science, Niigata University, 1-757, Asahimachi-dori, Chuo-ku, Niigata 951-8510, Japan

## ARTICLE INFO

## ABSTRACT

We analyzed hepatocellular carcinoma (HCC) with progenitor cell features using hepatic stem/progenitor cell marker neural cell adhesion molecule (NCAM). Approximately 8.3% of the operated HCC cases expressed NCAM, and 22.3% of the HCC patients had soluble NCAM levels >1000 ng/ml (the "highly soluble" NCAM group). Soluble NCAM status was a significant independent factor predictive of long-term survival in patients with HCC, and high levels of soluble NCAM were significantly related to intrahepatic metastasis. The 140-kDa NCAM isoform was specifically detected in the "highly soluble" NCAM group of HCC patients and its related signals are potential drug targets for NCAM+ HCC.

© 2011 Elsevier Ireland Ltd. All rights reserved.

## 1. Introduction

The two major primary liver cancers in adults are hepatocellular carcinoma (HCC) and cholangiocellular carcinoma (CC). In addition, mixed/combined forms of HCC and CC have been reported and their relationship with hepatic stem/progenitor cells is being actively analyzed [1,2]. Recently, further detailed immunohistochemical analysis of HCC using stem/progenitor cell markers revealed the existence of HCC in which a fraction of the tumor cells express stem/progenitor cell markers. These HCC are not otherwise recognizable by routine diagnosis by hematoxylin–eosin staining. These HCC are termed HCC with progenitor cell features and analysis of their prognosis revealed a high frequency of recurrence after hepatic resection and transplantation and a poor prognosis compared with conventional HCC [3–5]. Nevertheless, these tumors are clinically diagnosed and treated without distinguishing them from conventional HCC. Thus, the diagnosis of HCC with progenitor cell features without tumor biopsy and appropriate treatment are crucial for improving the prognosis of HCC patients. In the present study, we analyzed HCC with progenitor cell features using the previously reported stem/progenitor cell marker neural cell adhesion molecule (NCAM).

---

*Abbreviations:* HCC, hepatocellular carcinoma; NCAM, neural cell adhesion molecule; CK19, cytokeratin 19; IM, intrahepatic metastasis; CC, cholangiocellular carcinoma; FGFR, fibroblast growth factor receptor; NK, natural killer; GPI, glycosyl-phosphatidylinositol; DAPI, 4′ 6-diamidino-2-phenylindole; ELISA, enzyme-linked immunosorbent assay; PBS, phosphate-buffered saline; DMEM, Dulbecco's modified Eagle medium; SDS–PAGE, sodium dodecyl sulfate–polyacrylamide gel electrophoresis; PVDF, polyvinylidene fluoride; FACS, fluorescence-activated cell sorter; PE, phycoerythrin; PCR, polymerase chain reaction; Fyn, Src-related tyrosine kinase p59$^{fyn}$; GAP43, growth-associated protein 43; FRS2, fibroblast growth factor receptor substrate 2; Rac-1, ras-related C3 botulinum toxin substrate 1; Cdc42, cell division cycle 42; GAPDH, glyceraldehydes-3-phosphate dehydrogenase; AFP, α-fetoprotein; PIVKA-II, protein induced by vitamin K absence II, PSA, polysialic acid; EMT, epithelial mesenchymal transition; TGF, transforming growth factor; PLC, phospholipase C.

* Corresponding author. Tel.: +81 25 227 2207; fax: +81 25 227 0776.

*E-mail address:* atsunori@med.niigata-u.ac.jp (A. Tsuchiya).

NCAM is a cell adhesion molecule that was originally detected in the study of neurons and that belongs to the immunoglobulin superfamily. NCAM can homophilically bind to another NCAM, resulting in a zipper-like formation, and can bind heterophilically to L1-CAM, fibroblast growth factor receptor (FGFR) and extracellular components such as chondroitin, sulfate proteoglycan, heparin sulfate proteoglycan, collagen and laminin [6]. The large number of NCAM-interacting partners suggests that NCAM possesses important functions. In the normal human body, a variety of cells or tissues express NCAM, including NK cells, neuroendocrine gland, the central and peripheral nervous system and cardiomyocytes [6]. In addition, NCAM is also expressed by a variety of malignant cells such as neuroblastoma [7], rhabdomyosarcoma [8,9], small-cell lung cancer [10] and brain tumors [7], as well as by multiple myeloma [11] and acute myeloid leukemia [12]. The extracellular part of NCAM consists of five immunoglobulin-like domains and two fibronectin type III-like domains. Alternative mRNA splicing results in three major isoforms: a 120-kDa NCAM isoform is connected by a glycosyl-phosphatidylinositol (GPI) anchor to the cell membrane and is predominantly expressed in normal and well-differentiated tissues. Isoforms of 140- and 180-kDa, which contain a transmembrane domain, are found predominantly in less differentiated and malignant cell types [6]. Intracellular signaling of 140-kDa and 180-kDa NCAM is well understood from the study of neurons. It is also known that these isoforms and their downstream signals are involved in FGFR and N-cadherin signaling, as well as neurite motility and outgrowth [13]. Furthermore, NCAM can be released to the serum as a soluble form of NCAM, which includes NCAM forms with or without transmembrane domains. These soluble NCAM forms arise by processes such as alternative splicing of NCAM1 transcripts and by enzymatic processing of extracellular domains at the cell membrane. Thus, soluble NCAM has the potential to identify NCAM-expressing cells [14].

NCAM is known as a stem/progenitor cell marker in liver and is expressed in ductular reactions of acute and chronic damaged livers [15]. We also reported that NCAM is expressed in a fraction of some HCC cell populations [16]. As a tumor marker, NCAM has a number of benefits compared with other markers: (1) NCAM is a cell surface marker; (2) NCAM has three isoforms, two of whose downstream signals have been elucidated in studies of other fields; and (3) NCAM can be detected as a soluble form of NCAM in serum. These properties suggested that NCAM may be a useful marker for the diagnosis and treatment of NCAM+ HCC. In this study we analyzed NCAM expression in cases of operated HCC as well as the frequency and clinical course of NCAM+ HCCs. The level of soluble NCAM was measured in the serum of HCC patients and its relationship to the prognosis and intrahepatic metastasis of HCC tumors was analyzed. We further identified the isoform of NCAM that can be specifically detected in patients with HCC and analyzed the growth and invasive ability of NCAM+ HCC cells and their related downstream signals in order to elucidate the reason for the poor prognosis of NCAM+ HCC.

## 2. Materials and methods

### 2.1. Specimen collection

We analyzed 60 cases of livers that were extirpated for resection of HCC. Paraffin-embedded liver tissues were analyzed after receiving IRB approval from Niigata University.

### 2.2. Staining

Liver tissue was fixed in 10% formalin and embedded in paraffin blocks. Four-micrometer sections were cut and mounted on silane-coated slides. For immunohistochemical analysis, after removing the paraffin, antigen retrieval was performed using antigen retrieval solution (BioGenex Laboratories, San Ramon, CA) for 15 min in a microwave oven. Endogenous peroxidase activity was blocked with 3% hydrogen peroxide in methanol (Wako, Osaka, Japan) for 10 min at room temperature, and sections were incubated overnight with the primary antibody, mouse anti-NCAM (123C3; Santa Cruz Biotechnology, Santa Cruz, CA), diluted in PBS. Slides were then stained using the Vectastain® ABC kit and DAB TRIS tablets (Muto Pure Chemicals, Tokyo, Japan). For immunocytochemical analysis, cells were washed with PBS and then fixed in methanol at −20 °C for 10 min. Anti-NCAM antibody (Santa Cruz Biotechnology) and Cy3-conjugated anti-mouse IgG antibody were employed as first and second antibodies, respectively. Nuclei were labeled with DAPI VECTASHIELD mounting medium for fluorescence analysis (Vector Laboratories, Inc., Burlingame, CA).

### 2.3. ELISA

The sera from 92 patients with HCC and 32 patients with chronic hepatitis C were measured. The cohort of the patients for ELISA was mostly different cohort of those for immunohistochemical analysis. All patients were followed up in our hospital. The sera were measured using the DuoSet® ELISA Development System for human NCAM1/CD56 (R&D Systems, Inc., Minneapolis, MN), according to the manufacturer's protocol. Briefly, the sera were diluted 1000-fold and pipetted into wells in a 96-well polystyrene microplate (R&D Systems, Inc.), the surface of which was coated with mouse anti-human NCAM1 antibody. After incubation, biotinylated goat anti-human NCAM1 was added to the well. After incubation and washing, streptavidin conjugated to horseradish-peroxidase was added, and finally, a color development step was performed. Absorbance was measured at 450 nm using the Biotrak visible plate reader (GE Healthcare Life Science, Buckinghamshire, UK). All samples were measured in duplicate.

### 2.4. Western blot analysis

The sera of four patients with HCC from the highly soluble-NCAM group, one patient with HCC from the minimally soluble-NCAM group, one patient with chronic

hepatitis, one patient with liver cirrhosis, and two people without disease was analyzed by western blotting. Three microliters of each serum was diluted with 30 μl of PBS and 30 μl of lysis buffer [150 mM NaCl, 1% Triton X-100, 10 mM Hepes (pH 7.49)] was added. Laemmli Sample Buffer (20 μl, Bio-Rad Laboratories, Hercules, CA) was then added to 20 μl of this mixture. The samples were separated by sodium dodecyl sulfate–polyacrylamide gel electrophoresis (SDS–PAGE) using 7.5% READY GELS J (Bio-Rad Laboratories) and were electroblotted onto polyvinylidene fluoride (PVDF) membranes (Immobilon-P, Millipore Corporation, Billerica, MA). After incubation with the primary anti-NCAM antibody (123C3; Santa Cruz Biotechnology), which binds all three isoforms, antibody-bound proteins were visualized using the ONE-HOUR Westerns™ kit (GenScript Corporation, Piscataway, NJ) according to the manufacturer's protocol.

### 2.5. MACS® and flowcytometry

Cultured JHH-6 cells were dissociated using cell dissociation buffer (Beckton Dickinson, San Jose, CA) for 30 min at 37 °C, and single cells were obtained. The resulting cells were incubated with phycoerythrin (PE)-conjugated mouse anti-human CD56 antibody (Beckton Dickinson) for 15 min on ice. After washing, the cells were analyzed using FACScan (Beckton Dickinson). Dissociated single cells were also used for the separation of NCAM+ and NCAM− cells within the JHH-6 cell population. The resulting cells were incubated with microbead-conjugated anti-human CD56 (Miltenyi Biotec, Inc., Auburn, CA) for 15 min. After washing, cells were separated using Midi MACS® (Miltenyi Biotec, Inc.) and LS columns (Miltenyi Biotec, Inc.) according to the manufacturer's protocol.

### 2.6. Cell culture

The HCC cell lines JHH-5, JHH-6, JHH-7, HLE and HLF were purchased from the Health Science Research Resources Bank, Osaka, Japan. JHH-5, JHH-6 and JHH7 cells were maintained in William's E medium containing 10% fetal bovine serum and penicillin/streptomycin (Sigma–Aldrich, Inc., St. Louis, MO), and the HLE and HLF cell lines were maintained with DMEM containing 10% fetal bovine serum and penicillin/streptomycin. For the growth assay, $4.5 \times 10^5$ NCAM+ or NCAM− JHH-6 cells were cultured for 3 days and, then counted. The invasion ability of separated NCAM+ and NCAM− cells was compared in an invasion assay that employed the BD Biocoat™ Matrigel™ Invasion Chamber (Beckton Dickinson), according to the manufacturer's protocol.

### 2.7. Real-time PCR

Total RNA was isolated from the NCAM+ and the NCAM− JHH-6 cells using the RNeasy Mini kit (Qiagen, Chatsworth, CA) according to the manufacturer's protocol; 1 μg of total RNA was used as a template for the synthesis of cDNA using the Transcriptor First Strand cDNA Synthesis kit (Roche Applied Science, Mannheim, Germany). Aliquots of cDNA samples were subjected to real-time PCR using a LightCycler

System (Roche Applied Science). The TaqMan probe and primer sets for Src-related tyrosine kinase p59$^{fyn}$ (Fyn; assay identification number Hs00176628_m1), growth-associated protein 43 (GAP43; assay identification number Hs00967138_m1), fibroblast growth factor receptor substrate 2 (FRS2; assay identification number Hs01565776_m1), N-cadherin (assay identification number Hs00169953_m1), ras-related C3 botulinum toxin substrate 1 (Rac-1; assay identification number Hs00251654_m1) and cell division cycle 42 (Cdc42; assay identification number Hs00741586_m1) were used for the TaqMan Gene Expression Assay (Applied Biosystems, Foster City, CA). PCR conditions were as follows: 95 °C for 10 min followed by 45 cycles of 95 °C for 10 s, 60 °C for 30 s, and 72 °C for 1 s. The results were normalized to the level of mRNA for human glyceraldehyde-3-phosphate dehydrogenase (GAPDH). Gene expression measurements were performed in triplicate. These mRNA samples were from separated MACS isolations of the JHH-6 cells.

### 2.8. Statistics

Statistical analyses were performed using the SPSS 15.0 software package (SPSS Japan Inc., Tokyo, Japan) and GraphPad Prism 5 software (GraphPad Software, Inc., La Jolla, CA). Multivariate analysis of prognostic factors of patients with HCC was performed using a Cox's proportional-hazard model. The overall survival of patients with HCC was compared using the Kaplan–Meier method. A log-rank test was used to test the equality of long-term survival between groups. The serum levels of soluble NCAM were assessed for association with intrahepatic metastasis using Fisher's exact test. The results of the growth and invasion assays of JHH-6 and real-time PCR were assessed using the Mann–Whitney test. Differences were considered significant when the P value was less than 0.05.

### 3. Results

#### 3.1. Approximately 8.3% of operated hepatocellular carcinoma expressed NCAM

We first immunohistochemically analyzed NCAM expression in 60 cases of previously operated HCC to confirm the frequency of NCAM+ HCC. Of the 60 cases of HCC, 5 cases (8.3%) expressed NCAM (Fig. 1); and their clinical characteristics are described in Table 1. NCAM+ HCC cells formed a cluster from that NCAM+ cells extended into the NCAM− HCC area. By analyzing the clinical features of the NCAM+ HCCs, several interesting points were noted. First, all cases involved men. Second, despite the close follow-up, four of five cases detected were >35 mm in diameter. Third, all cases possessing NCAM+ cancer cells were moderately differentiated HCCs. Fourth, contrast-enhanced computed tomography revealed that four of five cases (excluding case 4) showed an early hyper-enhanced arterial vascularization followed by enhanced hypoattenuation (wash-out) in the late phase of imaging (data not shown). These results revealed that typical clinical imaging of HCCs included NCAM+ HCCs. Fifth, in the cases we examined no relationship was seen between the frequency of NCAM+ cancer cells and the serum levels of AFP or PIVKA-II. Sixth, portal invasion was seen in three of five cases. Seventh, these NCAM+ HCC cases included relatively small tumor cells with high nuclear/cytoplasmic ratios. Because only 5 NCAM+ HCC cases were analyzed and were not compared in detail with the results of NCAM− HCC cases, accurate prognosis was not possible. However, based
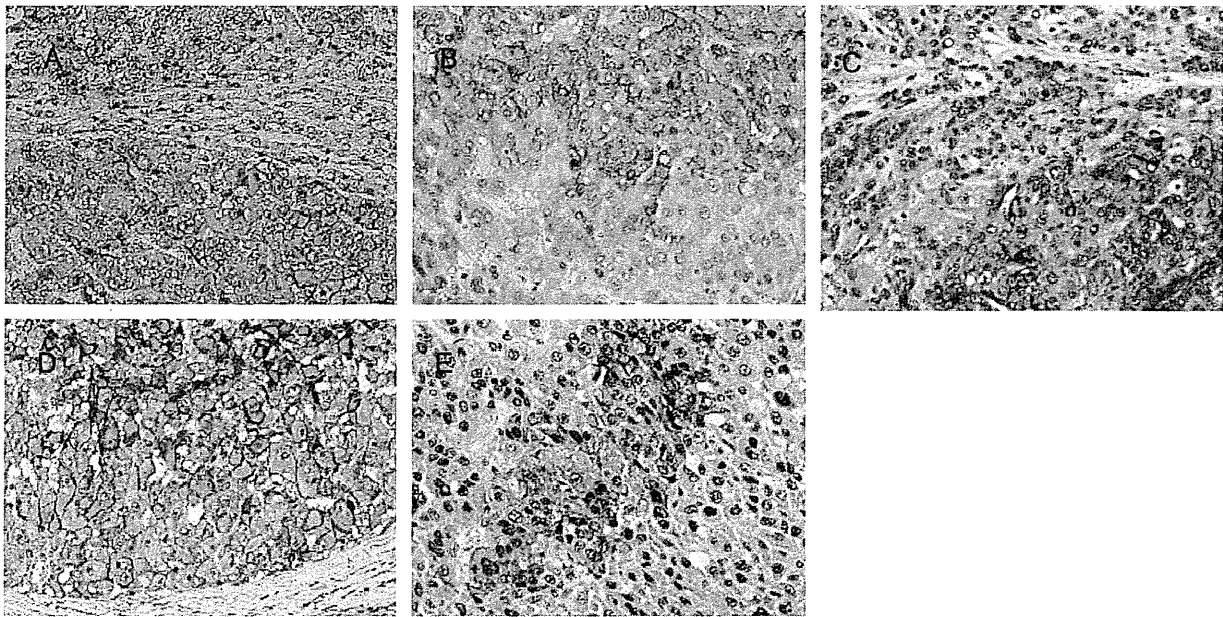
**Fig. 1.** NCAM+ cells in HCC. Immunohistochemical analysis of five cases of NCAM+ HCC is shown (A–E, magnification 200×). NCAM+ cells appear to form a cluster, from which NCAM+ cells extend into the NCAM–HCC area.

**Table 1**
Clinical characteristics of the patients with NCAM+ HCC.

| Case | Age | Sex | Diagnosis | Tumor lesion and size | Degree of differentiation | NCAM+ cells (%) | AFP | PIVKA | Pre-operative remarks | Pathological portal vein invasion | Survival time |
|------|-----|-----|-----------|------------------------|---------------------------|------------------|-----|-------|------------------------|-----------------------------------|---------------|
| 1 | 78 | M | HCC LC(NBNC) | S6-7, 40 mm | mod | >5 | 15 | 20 | Post portal vein embolization | + | 71 days dead |
| 2 | 70 | M | HCC, HCV | S5, 20 mm | mod | >5 | 10.9 | 24 | Post IFN (SVR), SMANCS i.a. | – | 30 months alive |
| 3 | 73 | M | HCC, HCV | S6-7, 52 mm | mod | >5 | 105 | ND | Post IFN | + | 80 days dead |
| 4 | 60 | M | HCC, HBV | S5, 35 mm | mod | >5 | 548 | ND | IFN, Lamivudin, Entecavir | + | 14 months dead |
| 5 | 75 | M | HCC, HBV | S8, 55 mm | mod | <5 | 37.5 | 465 | Lamivudin + Adefovir | – | 29 months alive |

NBNC; non-B (HBV) non-C (HCV), mod; moderately differentiated hepatocellular carcinoma, SVR; sustained virological response, SMANCS; styrene maleic acid neucarzinostatin, IFN; interferon.

on the above findings, we speculated that the prognosis of NCAM+ HCC is poor. To confirm our speculation, the following experiments were conducted.

### 3.2. The serum level of soluble NCAM is an independent factor related to the prognosis of HCC

To examine the presence of NCAM+ HCC without performing a liver biopsy, we measured soluble NCAM by ELISA using the serum from 92 patients with HCC and from 32 patients with chronic hepatitis C (Fig. 2). The mean level of soluble NCAM in the serum of patients with HCC ($725.0 \pm 327.8$ ng/ml) was higher than that in patients with chronic hepatitis C ($532.7 \pm 231.7$ ng/ml). When the patients were divided to highly soluble and minimally soluble NCAM groups (>1000 ng/ml and <1000 ng/ml of soluble NCAM, respectively), it was obvious that more patients with HCC (22.8%) than patients with chronic hepatitis C (6.3%) belonged to the highly soluble-NCAM group. Multivariate analysis using a Cox's proportional-hazard model revealed that NCAM status ($P < 0.047$) was a significant independent factor predictive of long-term survival in patients with HCC in addition to the Child-Pugh score, $\alpha$-feto-protein, and TNM stage (Table 2). We also compared the overall survival

period of minimally soluble and highly soluble-NCAM groups from first detection of HCC using the Kaplan–Meier method (Fig. 3A). The survival period of the highly soluble-NCAM group was significantly shorter than that of the minimally soluble-NCAM group (log-rank test; $P < 0.0015$).

### 3.3. Soluble NCAM is related to intrahepatic metastasis of HCC, but early detection of NCAM+ HCC is difficult when based on soluble NCAM alone

When we analyzed the clinical course of NCAM+ HCC, we found that many patients in the highly soluble-NCAM group had intrahepatic metastasis (IM). In fact, the frequency of IM in the highly soluble-NCAM group (81.0%) was higher than that in the minimally soluble-NCAM group (45.7%) (Fig. 3B). To examine the relationship between high serum levels of soluble NCAM and IM, Fisher's exact test was performed. This test confirmed that high serum levels of soluble NCAM were related to IM ($P < 0.0114$). Next, to determine whether soluble NCAM can be used as a marker for the detection of HCC at early stages, the TNM stage of the highly soluble HCC group was evaluated. because the number of patients in the highly soluble-NCAM groups increases after stage II (Fig. 4A), this limits the detection of NCAM+ HCC at an early stage based strictly on soluble NCAM levels.
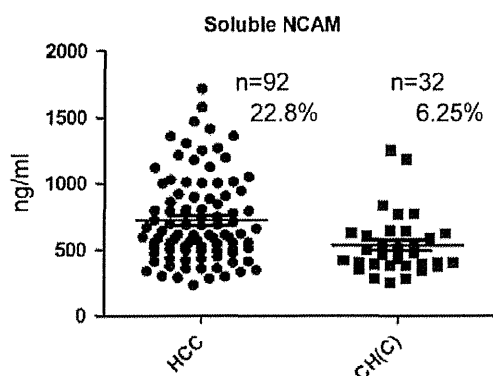
**Fig. 2.** Serum levels of soluble NCAM in patients with HCC and in patients with chronic hepatitis C (CH (C)). Serum NCAM was measured using an ELISA. The mean level of soluble NCAM and the percentage of patients that expressed high levels of soluble NCAM (22.8%, patients with HCC; 6.25%, patients with CH (C)) were higher in patients with HCC than in patients with CH (C).

**Table 2**
Multivariate analysis of predictive factors of long term survival in patients with HCC.

| Variable | Hazard ratio (95% CI) | P value |
|---|---|---|
| Gender (male/female | 0.659 (0.236–1.839) | 0.425 |
| Age (<65/⩾) | 0.554 (0.175–1.748) | 0.313 |
| Etiology (C/B/others) | 1.340 (0.717–2.504) | 0.359 |
| Child-Pugh (A/B, C) | 3.029 (1.262–7.269) | 0.013 |
| AFP (Log ng/ml) | 1.406 (0.999–1.979) | 0.050 |
| DCP (Log mA U/ml) | 1.005 (0.576–1.754) | 0.985 |
| NCAM (<1000/⩾1000 ng/ml) | 2.595 (1.011–6.666) | 0.047 |
| TNM stage (1/2/3/4) | 2.114 (1.189–3.754) | 0.011 |

Cox's proportional-hazard model.

*3.4. The 140-kDa NCAM isoform was highly expressed in the highly soluble-NCAM group*

To find a marker that is specifically expressed in NCAM+ HCC and to resolve the problem posed by the fact that soluble NCAM alone is not a good marker for the early detection of NCAM+ HCC, we examined the serum isoforms of soluble NCAM by western blot analysis. We examined the sera from four patients with HCC from the highly soluble-NCAM group

(Fig. 4B, a–d), one patient with HCC from the minimally-soluble NCAM group (Fig. 4B, e), one patient with chronic hepatitis (Fig. 4B, f), one patient with liver cirrhosis (Fig. 4B, g), and two individuals without disease (Fig. 4B, h–i). NCAM bands at 120-kDa were detected in all samples, at varying intensity. The NCAM bands of 140-kDa were only detected in three of four patients with HCC in the highly soluble-NCAM group (Fig. 4B, a, b and d). However, the NCAM band at 140-kDa was not detected in one patient with HCC, who was in the highly soluble-NCAM group (Fig. 4B, c). The clinical course of this patient revealed that the patient had neurological disease (demyelinating disorder) however viable HCC was very small (TNM stage I). High levels of soluble NCAM in patients with neurological disease are well known [14]. Thus, we concluded that high levels of soluble NCAM in this patient was mainly due to neurological disease rather than HCC. These results revealed that 140-kDa NCAM isoform was only detected in HCC patients without neurological disease and strongly suggested that the 140-kDa NCAM isoform was derived from NCAM+ HCC. The NCAM band at 180-kDa could not be detected in any sample (Fig. 4B). Thus, we concluded that the 140-kDa NCAM isoform might be useful as a specific marker of NCAM+ HCC.

*3.5. The JHH-6 cell line expresses NCAM, and NCAM+ cells have high growth potential and invasive ability*

To examine NCAM+ HCC in more detail, we looked for HCC cell lines that express NCAM. We immunostained five HCC cell lines (JHH-5, JHH-6, JHH-7, HLE and HLF) and found that JHH-6 cells include NCAM+ cells (Fig. 5A). JHH-6 cells were previously reported to have a higher metastatic ability than JHH-5 and JHH-7 cells when they were implanted into the liver [17]. Flow cytometric analysis revealed that approximately 70% of the JHH-6 cells expressed NCAM (Fig. 5B). We then separated JHH-6 cell lines to two populations: an NCAM+ cell-enriched group and an NCAM− cell-enriched group (approximately 90% pure populations) and compared their growth and invasive abilities (Fig. 5B). Both the growth and the invasive ability of the NCAM+ cell-enriched group was higher than those of the NCAM− enriched group (P < 0.05; P < 0.009, respectively) (Fig. 5C and D). These data support the adverse biological behavior and poor clinical course of NCAM+ HCC.

*3.6. The 140-kDa NCAM and its downstream signals may affect the clinical course of NCAM+ HCC and may be related to FGFR and its downstream signals*

Finally, to elucidate intracellular signals that are specifically expressed in NCAM+ cells we compared the mRNA of enriched JHH-6 NCAM+ and NCAM− cells using real-time PCR. We examined the mRNA level of the following signals: Fyn; a downstream signal of 140-kDa NCAM, GAP43; a downstream signal of 180-kDa NCAM, FRS2; a downstream signal of FGFR, N-cadherin, Rac-1 and Cdc42; signals downstream of N-cadherin. All of these signals were well known from the study of neuron, thus we confirmed them. The Fyn and FRS2 mRNA levels in enriched NCAM+ cells were significantly higher than those of enriched
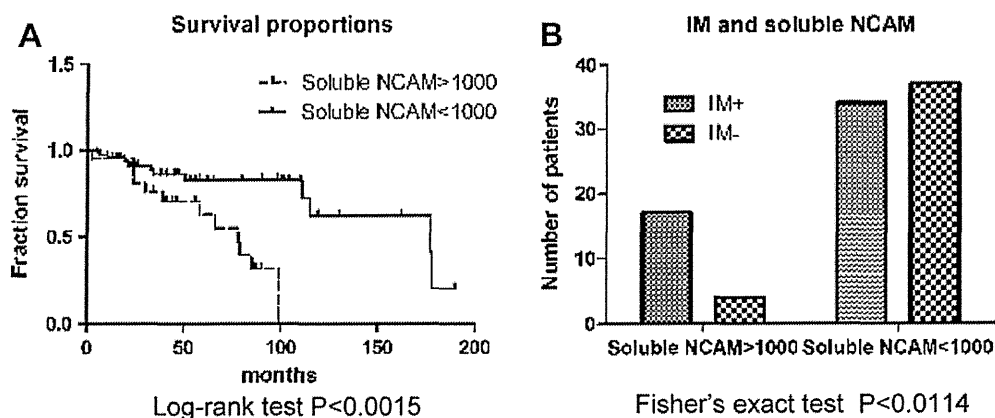


**Fig. 3.** Relationship between serum soluble NCAM levels and survival (A) and intrahepatic metastasis (IM) (B). (A) Kaplan–Meier analysis of survival revealed that the survival period of the highly soluble-NCAM group was significantly shorter than that of the minimally soluble-NCAM group (log-rank test; P < 0.0015). (B) The frequency of IM in the highly soluble-NCAM group was obviously higher than that in the minimally soluble NCAM group. High levels of serum soluble NCAM were related to IM, as assessed using Fisher's exact test (P < 0.0114).
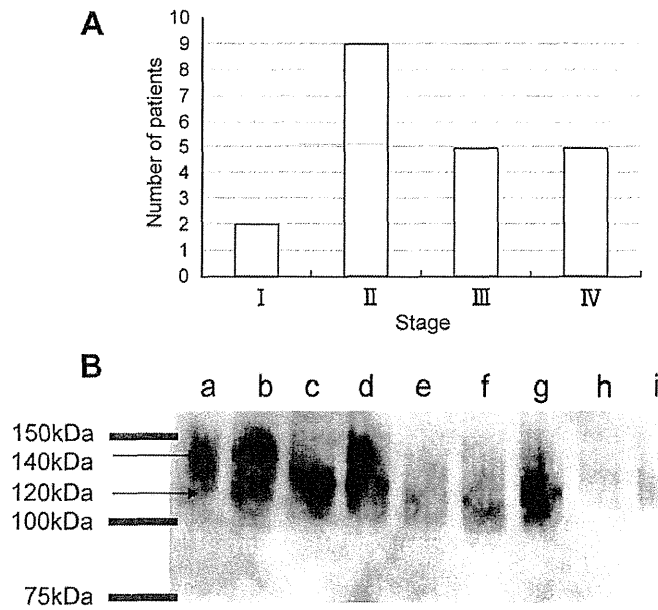
Fig. 4. TNM stage of the patients in the highly soluble-NCAM group (A), and western blot analysis of serum soluble NCAM isoforms (B). (A) Most of the patients in the highly soluble-NCAM group were classified as TNM stage II or higher. (B) Western blotting of NCAM isoforms in the sera of patients with HCC in the highly soluble-NCAM group (a–d), and the minimally soluble NCAM group (e), and of the serum of a patient with chronic hepatitis (f), of patients with liver cirrhosis (g) or the sera of two healthy people (h and i). The 140-kDa NCAM band could only be detected in three of four patients with HCC in the highly soluble-NCAM group (a, b and d). In this group, one patient, who had neurological disease (demyelinating disorder), did not express the 140-kDa NCAM band (c).

NCAM− cells (Fig. 6A and C). We could not detect GAP43 mRNA (Fig. 6B). The mRNA levels of N-cadherin and its downstream signals Rac-1 and Cdc42 were relatively higher in the enriched NCAM+ group, but this difference was not significant (Fig. 6D–F). These data are consistent with our finding that the 140-kDa NCAM can be detected in the serum from the highly soluble-NCAM group. All of these results suggested that the 140-kDa NCAM and its downstream signals affect the clinical course of NCAM+ HCC and are related to FGFR and its downstream signals as the research in neuron indicated [13].

## 4. Discussion

In this study, we analyzed HCC with progenitor cell features using a previously reported hepatic stem/progenitor cell marker, NCAM. Recent detailed immunohistochemical analysis using stem/progenitor cell markers such as CK7 [18], CK19 [3] and OV6 [19] revealed that a substantial number of HCCs include a fraction of cells that express stem/progenitor cell markers. The reports regarding CK19+ HCC are worthy of special mention. Roskams et al. reported that CK19+ HCC (present in more than 5% of tumor cells) had a higher rate of tumor recurrence after liver transplantation [3]. Wu et al. reported a significantly shorter survival of patients with HCCs that expressed AE1–AE3 and CK19 without treatment [4]. Uenishi et al. reported that HCCs expressing CK7 and CK19 have a lower tumor-free survival rate after curative resection and also mentioned that CK19 expression was an independent predictor of postoperative recurrence [5]. Furthermore, Ding et al. observed that the overexpression of CK19 correlates with HCC metastasis [20]. Although the analyses in these reports were slightly different, they all highlight that the prognosis of CK19+ HCC is poor in comparison with conventional HCC. However, the reason for this poor prognosis has not been elucidated. Here, we analyzed NCAM expression in HCC with progenitor cell features.

The use of NCAM as a marker has three advantages compared to the use of CK19. First, NCAM is a cell surface marker; thus, NCAM+ cells can be easily analyzed by flow cytometry. Additionally, NCAM+ cells can be enriched by MACS and these enriched cells can be analyzed using a number of techniques such as growth in culture and PCR. Second, NCAM can be detected in serum as soluble NCAM, and levels of soluble NCAM and the soluble NCAM isoform can be analyzed. Third, NCAM has been analyzed extensively in terms of its function in neurons; therefore, isoforms of NCAM as well as intracellular signals of NCAM and related receptors such as the FGFR are well known. We conducted double immunohistochemical analysis using CK19 and NCAM. Because both antibodies are derived from mice and thus detail analysis were difficult, these two antibodies detected at least similar cell populations. These results revealed that NCAM+ HCC in this study represented at least similar subset as the CK19+ HCC.

Our analysis revealed that the prognosis of previously operated NCAM+ HCC was not good and that the prognosis of the highly soluble-NCAM group was very poor. These data were similar to the results of the CK19+ HCC study. We were also able to analyze the clinical course of NCAM+ HCC by measurement of serum-soluble NCAM, which obviated the need to perform a liver biopsy. We also found that a high level of soluble NCAM was related to IM. Western blot analysis revealed that 140-kDa NCAM was specifically detected in patients with HCC in the highly soluble-NCAM group, and real-time PCR analysis revealed that NCAM+
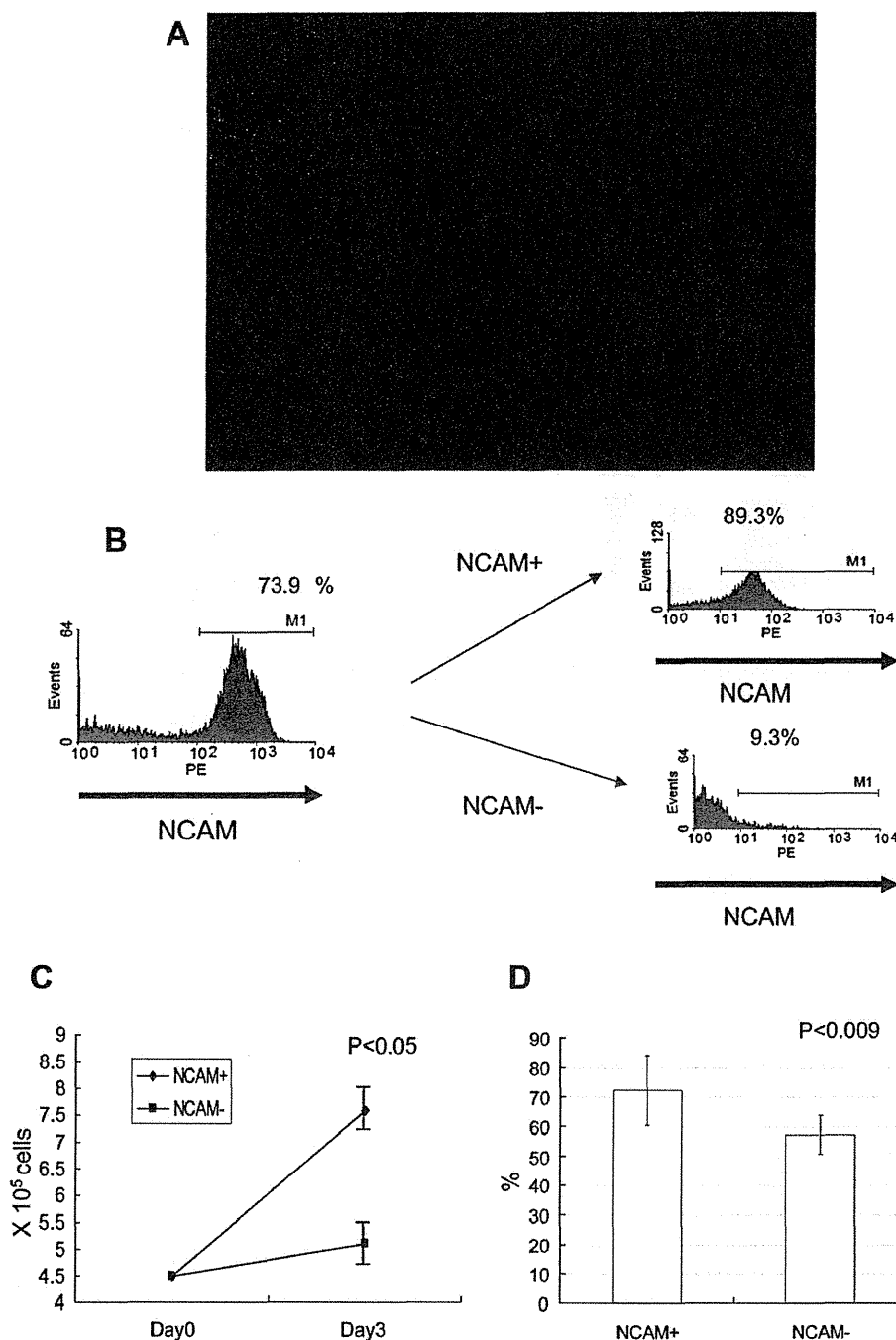
Fig. 5. Immunocytochemistry of JHH-6 cells using an anti-NCAM antibody (A), and analysis of the growth and invasive ability of NCAM+ and NCAM− cells (B and C). (A) NCAM+ cells (red) were included within the JHH-6 cell population. The nuclei were stained with DAPI (blue). (B) JHH-6 cells were separated to NCAM+ cells and NCAM− cells using MACS. Flowcytometric analysis indicated that the frequency of NCAM+ cells in the JHH-6 population was approximately 70%. JHH-6 cells were separated in two populations, an NCAM+ cell-enriched group and an NCAM− cell-enriched group (approximately 90% pure populations). (C) $4.5 \times 10^5$ cells each of the separated NCAM+ and NCAM− JHH-6 cells were cultured for 3 days and were then counted. (D) Invasive ability was assayed by examining the frequency of cells that invaded Matrigel in an invasion chamber compared with cells that invaded in the control chamber. The NCAM+ cells showed higher growth (Mann–Whitney test; $P < 0.05$) and more invasive (Mann–Whitney test; $P < 0.009$) ability than the NCAM− cells.

cells in the JHH-6 cell line expressed higher levels of mRNA that encodes signals downstream of 140-kDa NCAM and FGFR, as compared to NCAM− cells. Furthermore NCAM+ JHH-6 cells exhibit more rapid growth and greater invasive ability than NCAM− cells. All of these data support the idea that NCAM+ HCC has a poor prognosis. This is the first study to reveal a reason for the poor prognosis of HCC with progenitor features.

Although the prognosis of HCC with progenitor cell features is poor, the association between NCAM expression and patient prognosis seems to be dependent on tumor origin. Upregulation of NCAM expression correlates with
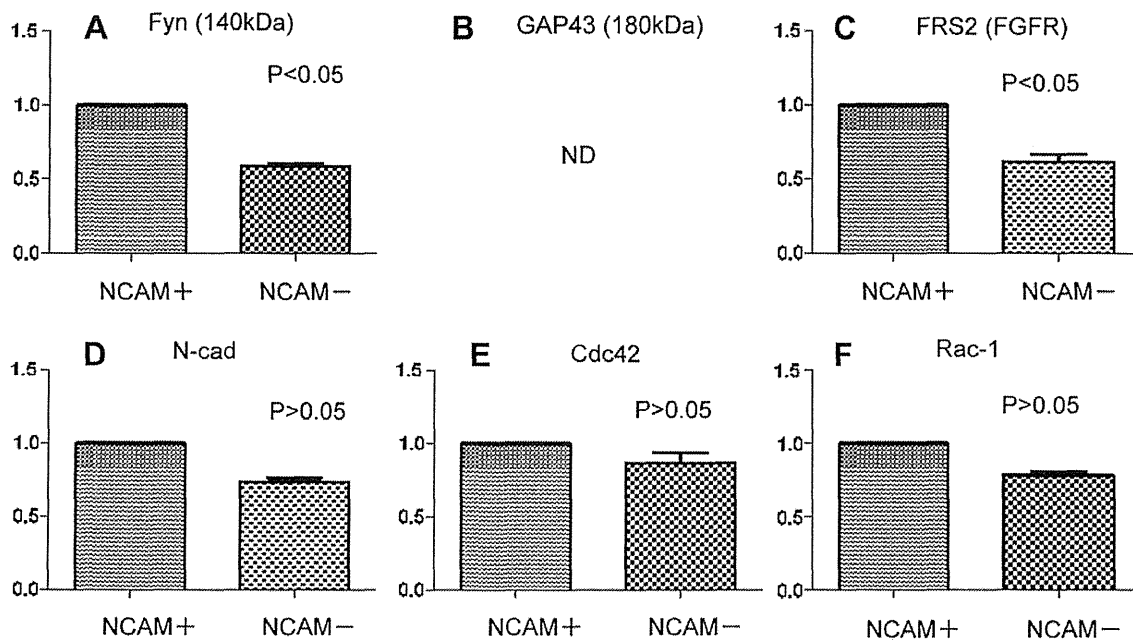
**Fig. 6.** Real-time PCR analysis of the mRNA expression of selected signaling molecules in NCAM+ and NCAM− cells. The mRNA levels of Fyn and FRS2, signals downstream of 140-kDa NCAM and FGFR, respectively, were significantly higher in NCAM+ cells than in NCAM− cells (Mann–Whitney test; $P < 0.05$). The mRNA levels of N-cadherin (N-cad) and its downstream signals Cdc42 and Rac-1 were higher in NCAM+ cells than in NCAM− cells, but the differences were not significant. The mRNA of GAP43, which is downstream of 180-kDa NCAM, was not detected (ND). Each mRNA level is expressed relative to that of GAPDH in the same sample.

poor prognosis in melanoma, acute myeloid leukemia and HCC, whereas the downregulation of NCAM is associated with a poor outcome in colon cancer and glioma [21]. Recently, it has been suggested that post-translational glycosylation with polysialic acids (PSA) plays a prominent role in cell adhesion [22,23]. Current data suggest that PSA plays an important role as an antagonist of native NCAM function [22]. Further analysis including PSA–NCAM expression may elucidate the difference between the prognoses of different tumors that express NCAM.

In our study, we suggest that 140-kDa NCAM and its downstream signals are important for adverse biological behavior. Recently, using mammary gland epithelial cells and breast cancer cells, Lehembre et al. reported an interesting change in NCAM signaling during tumor development [24]. The authors reported that the induction of the epithelial mesenchymal transition (EMT) via TGF-β or following cadherin loss not only causes NCAM-mediated weakening of cell–cell adhesion, but also induces the formation and dynamic turnover of focal adhesions. These events are accompanied by elevated NCAM expression, which leads to altered signal complexes. Specifically, NCAM binding to PLCγ and contactin is diminished whereas NCAM complexes with Fyn (downstream of 140-kDa NCAM) increase. These signaling changes are linked to the induction of the more mesenchymal and migratory phenotype that is associated with aggressive cancers of epithelial origin [24,25]. In our study, the 140-kDa isoform of NCAM was observed to be expressed in the highly soluble-NCAM group. The biological behavior of this group is clinically adverse; thus, our reports are consistent with the previous report. These data suggest

that NCAM+ HCC cells may develop a mesenchymal-like migratory/invasive phenotype.

Regarding the treatment of NCAM+ HCC because NCAM is a cell surface marker and because it can modulate growth and invasion, NCAM-targeted therapy would be an attractive therapy. Of the spectrum of existing anti-NCAM compounds, radioimmunoconjugates and immunotoxins represent the most advanced and successful therapeutic strategies [6]. Recently, NCAM-targeted liposomes loaded with doxorubicin and lipophilic gadolinium (Gd) derivatives were generated for the treatment of Kaposi's sarcoma. This liposome strategy may provide specific drug delivery to, as well as facilitate imaging of, NCAM-expressing tumors. The treatment of mice with NCAM-targeted liposomes resulted in an enhanced therapeutic effect and reduced toxicity compared to treatment with nontargeted liposomes [26]. In the human liver, transarterial chemotherapy is routinely used for HCC therapy; we could thereby treat NCAM+ HCC cells more specifically. Downstream signals of 140-kDa NCAM and of FGFR are also potential targets of molecular-targeted drugs. Combination therapy consisting of NCAM-targeted therapy and the currently existing therapy may be an efficient treatment for cancer cells.

Therefore, NCAM may not only be a useful marker for the diagnosis of NCAM+ HCC but may also be an attractive therapeutic target for NCAM+ HCC.

## Conflict of interest

The authors declare that they have no conflict of interest.

## Acknowledgments

## References

[1] M. Kojiro, Histopathology of liver cancers, Best Pract. Res. Clin. Gastroenterol. 19 (2005) 39–62.

[2] M. Komuta, B. Spee, S. Vander Borght, R. De Vos, C. Verslype, R. Aerts, H. Yano, T. Suzuki, M. Matsuda, H. Fujii, V.J. Desmet, M. Kojiro, T. Roskams, Clinicopathological study on cholangiolocellular carcinoma suggesting hepatic progenitor cell origin, Hepatology 47 (2008) 1544–1556.

[3] T. Roskams, Liver stem cells and their implication in hepatocellular and cholangiocarcinoma, Oncogene 25 (2006) 3818–3822.

[4] P.C. Wu, V.C. Lai, J.W. Fang, M.A. Gerber, C.L. Lai, J.Y. Lau, Hepatocellular carcinoma expressing both hepatocellular and biliary markers also expresses cytokeratin 14, a marker of bipotential progenitor cells, J. Hepatol. 31 (1999) 965–966.

[5] T. Uenishi, S. Kubo, T. Yamamoto, T. Shuto, M. Ogawa, H. Tanaka, S. Tanaka, K. Kaneda, K. Hirohashi, Cytokeratin 19 expression in hepatocellular carcinoma predicts early postoperative recurrence, Cancer Sci. 94 (2003) 851–857.

[6] M. Jensen, F. Berthold, Targeting the neural cell adhesion molecule in cancer, Cancer Lett. 258 (2007) 9–21.

[7] S.P. Bourne, K. Patel, F. Walsh, C.J. Popham, H.B. Coakham, J.T. Kemshead, A monoclonal antibody (ERIC-1), raised against retinoblastoma, that recognizes the neural cell adhesion molecule (NCAM) expressed on brain and tumours arising from the neuroectoderm, J. Neurooncol. 10 (1991) 111–119.

[8] G. Mechtersheimer, M. Staudter, P. Moller, Expression of the natural killer cell-associated antigens CD56 and CD57 in human neural and striated muscle cells and in their tumors, Cancer Res. 51 (1991) 1300–1307.

[9] W.M. Molenaar, F.L. Muntinghe, Expression of neural cell adhesion molecules and neurofilament protein isoforms in skeletal muscle tumors, Hum. Pathol. 29 (1998) 1290–1293.

[10] T. Hirano, S. Hirohashi, T. Kunii, M. Noguchi, Y. Shimosato, Y. Hayata, Quantitative distribution of cluster 1 small cell lung cancer antigen in cancerous and non-cancerous tissues, cultured cells and sera, Jpn. J. Cancer Res. 80 (1989) 348–355.

[11] P. Tassone, A. Gozzini, V. Goldmacher, M.A. Shammas, K.R. Whiteman, D.R. Carrasco, C. Li, C.K. Allam, S. Venuta, K.C. Anderson, N.C. Munshi, In vitro and in vivo activity of the maytansinoid immunoconjugate huN901-N2'-deacetyl-N2'-(3-mercapto-1-oxopropyl)-maytansine against CD56+ multiple myeloma cells, Cancer Res. 64 (2004) 4629–4636.

[12] S. Ikushima, T. Yoshihara, T. Matsumura, S. Misawa, Y. Morioka, S. Hibi, S. Imashuku, Expression of CD56/NCAM on hematopoietic malignant cells. A useful marker for acute monocytic and megakaryocytic leukemias, Int. J. Hematol. 54 (1991) 395–403.

[13] S.M. Hansen, V. Berezin, E. Bock, Signaling mechanisms of neurite outgrowth induced by the cell adhesion molecules NCAM and N-cadherin, Cell. Mol. Life Sci. 65 (2008) 3809–3821.

[14] T. Secher, Soluble NCAM, Neurochem. Res. (2008).

[15] H. Zhou, L.E. Rogler, L. Teperman, G. Morgan, C.E. Rogler, Identification of hepatocytic and bile ductular cell lineages and candidate stem cells in bipolar ductular reactions in cirrhotic human liver, Hepatology 45 (2007) 716–724.

[16] A. Tsuchiya, H. Kamimura, M. Takamura, S. Yamagiwa, Y. Matsuda, Y. Sato, M. Nomoto, T. Ichida, Y. Aoyagi, Clinicopathological analysis of CD133 and NCAM human hepatic stem/progenitor cells in damaged livers and hepatocellular carcinomas, Hepatol. Res. 39 (2009) 1080–1090.

[17] K. Murakami, R. Sakukawa, T. Ikeda, T. Matsuura, S. Hasumura, S. Nagamori, Y. Yamada, I. Saiki, Invasiveness of hepatocellular carcinoma cell lines: contribution of membrane-type 1 matrix metalloproteinase, Neoplasia 1 (1999) 424–430.

[18] P. Van Eyken, R. Sciot, A. Paterson, F. Callea, M.C. Kew, V.J. Desmet, Cytokeratin expression in hepatocellular carcinoma: an immunohistochemical study, Hum. Pathol. 19 (1988) 562–568.

[19] P.Y. Zhuang, J.B. Zhang, X.D. Zhu, W. Zhang, W.Z. Wu, Y.S. Tan, J. Hou, Z.Y. Tang, L.X. Qin, H.C. Sun, Two pathologic types of hepatocellular carcinoma with lymph node metastasis with distinct prognosis on the basis of CK19 expression in tumor, Cancer 112 (2008) 2740–2748.

[20] S.J. Ding, Y. Li, Y.X. Tan, M.R. Jiang, B. Tian, Y.K. Liu, X.X. Shao, S.L. Ye, J.R. Wu, R. Zeng, H.Y. Wang, Z.Y. Tang, Q.C. Xia, From proteomic analysis to clinical significance: overexpression of cytokeratin 19 correlates with hepatocellular carcinoma metastasis, Mol. Cell. Proteomics 3 (2004) 73–81.

[21] P.B. Campodonico, E.D. de Kier Joffe, A.J. Urtreger, L.S. Lauria, J.M. Lastiri, L.I. Puricelli, L.B. Todaro, The neural cell adhesion molecule is involved in the metastatic capacity in a murine model of lung cancer, Mol. Carcinog. 49 (2010) 386–397.

[22] E. Gascon, L. Vutskits, J.Z. Kiss, The role of PSA–NCAM in adult neurogenesis, Neurochem. Res. (2008).

[23] M. El Maarouf, U. Rutishauser, Use of PSA–NCAM in repair of the central nervous system, Neurochem. Res. (2008).

[24] F. Lehembre, M. Yilmaz, A. Wicki, T. Schomber, K. Strittmatter, D. Ziegler, A. Kren, P. Went, P.W. Derksen, A. Berns, J. Jonkers, G. Christofori, NCAM-induced focal adhesion assembly: a functional switch upon loss of E-cadherin, EMBO J. 27 (2008) 2603–2615.

[25] M.C. Frame, G.J. Inman, NCAM is at the heart of reciprocal regulation of E-cadherin- and integrin-mediated adhesions via signaling modulation, Dev. Cell 15 (2008) 494–496.

[26] C. Grange, S. Geninatti-Crich, G. Esposito, D. Alberti, L. Tei, B. Bussolati, S. Aime, G. Camussi, Combined delivery and magnetic resonance imaging of neural cell adhesion molecule-targeted doxorubicin-containing liposomes in experimentally induced Kaposi's sarcoma, Cancer Res. 70 (2010) 2180–2190.

# Failure to Achieve 2-log₁₀ Viral Decrease in First Four Weeks of Peg-IFNα-2b Plus Ribavirin Therapy for Chronic Hepatitis C with Genotype 1b and High Viral Titer is Useful in Predicting Non-response: Evaluation of Response-guided Therapy

Shogo Ohkoshi[1], Satoshi Yamagiwa[1], Masahiko Yano[1], Hiromichi Takahashi[1], Yoh-hei Aoki[2],
Nobuo Waguri[3], Kentaro Igarashi[3], Soh-ichi Sugitani[4], Tohru Takahashi[5],
Tohru Ishikawa[6], Tomoteru Kamimura[6], Hiroto Wakabayashi[7], Toshiaki Watanabe[8],
Yasunobu Matsuda[1] and Yutaka Aoyagi[1]

[1]Gastroenterology and Hepatology, Graduate School of Medical and Dental Sciences, Niigata University, Japan
[2]Shibata Hospital, Shibata-city, Japan
[3]Niigata Municipal Hospital. Niigata-city, Japan
[4]Tachikawa General Hospital, Nagaoka-city, Japan
[5]Uonuma Hospital, Uonuma-city, Japan
[6]Sai-sei-kai Second Hospital, Niigata-city, Japan
[7]Takeda General Hospital, Aizuwakamatsu-city, Japan
[8]Watanabe Clinic, Sanjyou-city, Japan
Corresponding author: Shogo Ohkoshi, M.D, Ph.D., Gastroenterology and Hepatology,
Graduate School of Medical and Dental Sciences Niigata University, 1-754 Asahimachi-dori,
Cyuo-ku, Niigata-city, 951-8122, Japan.
Tel: +80252272204, Fax: +80252270776, E-mail: okoshi@med.niigata-u.ac.jp

## ABSTRACT

**Background/Aims:** To clarify clinical parameters predicting sustained viral response (SVR) during 48 weeks pegylated-interferon (peg-IFN)α-2b plus ribavirin therapy for Japanese patients with chronic hepatitis C [CH(C)] genotype 1b and high viral titers.
**Methodology:** One hundred and fifty-one (151) patients receiving peg-IFNα-2b plus ribavirin therapy for 48 weeks were enrolled. SVR and clinical parameters were evaluated. The relationship between virological parameters (substitutions in the core and NS5A) and the degree of early viral decrease was also studied.
**Results:** Seventy (46.4%) patients achieved SVR (per protocol analysis). Negative predictive value (NPV) of <2-log₁₀ decrease after 4 weeks of therapy for SVR was 78.0%; similar to that for failing to achieve early viral response (EVR) at 12 weeks (82.2%).
**Conclusions:** Failure to achieve 2- log₁₀ decrease in the first 4 weeks may be an important predictor of non-SVR during 48 weeks of peg-IFNα-2b plus ribavirin therapy; thus, therapeutic plans should be reassessed at that point.

## INTRODUCTION

Therapeutic efforts to eradicate hepatitis C virus (HCV) have made outstanding progress via pegylated-interferon (peg-IFN)α-2b plus ribavirin therapy. Sustained viral response (SVR) is achieved in about 50% of chronic hepatitis C [CH(C)] patients, even with genotype 1 and high viral titers (1-3). However, there remain a substantial number of patients who do not benefit from this therapy.

Because IFN-based therapy is expensive and is associated with various side effects (4-6), it is important to predict clinical and virological param-

eters that influence anti-viral response prior to treatment (7-9). The number of amino acid substitutions in interferon sensitivity determining region (ISDR) of NS5A is known to be a good indicator of sustained viral response (SVR) (10, 11). Akuta *et al.* recently showed that amino acid substitutions in core 70 (R to Q) and 91 (L to M) are good predictors for viral response in peg-IFN plus ribavirin (12, 13). As host factors, serum chemokine (C-X-C) motif ligand 10 (CXCL10) levels have been reported to be useful in predicting SVR (14, 15), while additional host factors that are involved in therapy outcome have been identified by genome-wide screening

(16). However, it is still difficult to reliably predict SVR, even with these factors. Thus, the clinical significance of response-guided therapy is important.

Viral kinetic studies with IFN have shown that viral levels decay exponentially in the first period of therapy, and the degree of viral decline may predict therapeutic outcomes (17-22). To date, achievement of complete early viral response (cEVR; negative HCV RNA at 12 weeks) is the most important factor predicting SVR, and is widely accepted as a useful marker in response guided therapy for CH (C). There is a much higher probability of non-response (NR) if EVR is not obtained (17-22).

The aim of study is to clarify clinical parameters predicting SVR in peg-IFNα-2b plus ribavirin therapy. We particularly focused on viral response in the first 4 weeks and attempted to verify its importance in response-guided therapy in order to facilitate earlier reassessment of therapeutic plans.

## METHODOLOGY

### Patient population

One hundred and fifty-one CH(C) genotype 1b patients with high viral load, who received 48 weeks peg-IFNα-2b plus ribavirin therapy in our hospital or affiliated institutions, were analyzed in the present study. These patients were followed until 24 weeks after the completion of the treatment. Clinical parameters that determine treatment outcomes were analyzed. By performing this analysis we confirmed that viral decrease in the first 4 weeks was a good indicator in predicting SVR; thus, the association between virological factors and serum CXCL10 levels and 4-week viral response was prospectively analyzed in a new group of 75 patients. The studies were approved by the ethical committee of Niigata University, and carried out in accordance to the Declaration of Helsinki. Informed consent was obtained from all patients before enrollment.

### Treatment regimen

Patients received peg-IFNα-2b (Pegintron; Schering-Plough, Kenilworth, NJ, USA) at a dosage of 1.5μg/kg every week subcutaneously for 48 weeks. The dose was reduced when blood neutrophil and platelet (Plt) levels decreased below 750/mm$^3$ and 7.5x10$^4$/μL, respectively. Daily ribavirin (Rebetol, Schering-Plough) was given orally for 48 weeks and the dosage was adjusted according to weight (600mg for ≤60kg, 800mg for 60 to 80kg, 1000mg for >80kg). The dose was also reduced when hemoglobin (Hgb) levels decreased below 10g/dL. Blood samples were obtained every 4 weeks, and were analyzed for biochemical parameters, while HCV RNA titers were measured by quantitative RT-PCR (Amplicor monitor version 2, Roche Diagnostic Systems, CA, USA) or HCV RNA negativity was evaluated by qualitative RT-PCR (Amplicor, Roche), which has a higher sensitivity than the quantitative method (about 50 copies/mL). RVR (rapid viral response) and EVR were defined as undetectable HCVRNA after 4 and 12 weeks of therapy, respectively. SVR was defined as undetectable HCV RNA at 24 weeks after completion of treatment.

The second group of 75 patients for whom virological and serum CXCL10 analysis was performed were similarly treated. Because many of these patients have yet to complete the treatment or continue to be followed, viral decrease in the first 4 weeks instead of final therapy outcome was tentatively set as an endpoint.

### Virological analysis

HCV RNA was extracted from sera obtained from the second group of 75 patients using a kit (QIAamp Viral RNA Mini Kit; Qiagen, Tokyo, Japan). The 628-bp core fragment and the 573-bp NS5A region were amplified by nested PCR analysis. First- and second-round primer sequences were as follows: for core region, 5'-ACTGCCTGATAG-GGTGCTTG- 3'(forward, outer) and 5'-GTTGGAG-CAGTCGTTCGTGAC-3'(reverse, outer), 5'-AG-GTCTCGTAGACCGTGCAC-3'(forward, inner) and 5'-CATGGTATATCCCGGACGCGTT-3' (reverse, inner); and for ISDR of NS5A; 5'-TGGATGGAGT-GCGGTTGCACAGGTA- 3'(forward, outer) and 5'-TCTTTCTCCGTGGAGGTGGTATTGC-3'(reverse, outer), 5'-TGTAAAACGACGGCCAGTCAG-GTACGCTCCGGCGTGCA-3'(forward, inner) and 5'-CAGGAAACAGCTATGACCGGGGCCTTGG-TAGGTGGCAA-3' (reverse, inner) (11). First-round PCR was performed using SuperScript One-step RT PCR (Qiagen, Tokyo, Japan). The resultant RT-PCR products were subjected to a second-round PCR by using Platinum Taq DNA polymerase (Invitrogen, Tokyo, Japan) (23).

Amplicons were purified using a kit (MinElute PCR Purification Kit; Qiagen) and directly sequenced (Applied Biosystems, Tokyo, Japan). The sequences obtained were analyzed using Bio-Edit software (Carlsbad, CA). Serum CXCL10 levels were measured by Enzyme Linked Immunosorbent Assay (ELISA) (R&D Systems, Inc., Minneapolis, MN, USA).

### Statistical analysis

Fisher's exact test and the chi-square test were used to evaluate the parameters [age, gender, weight, body mass index (BMI), peg-IFN and ribavirin adherence, alanine aminotransferase (ALT), white blood cell count (WBC), Hgb, Plt and the number of core and ISDR substitutions] to determine therapy outcome. Cochran-Armitage test was used to evaluate the relationship between HCV titer and virus decreases in the first 4 weeks, and therapy outcome. Quantitative data were divided into two groups using the median to examine the differences. We conducted multivariate analysis using stepwise logistic regression on parameters which achieved $p<0.20$ on univariate analysis. Student's $t$-test was used to compare the mean values of the two groups. All analyses were performed using a statistical software package (SPSS version

5.0, SAS Institute Inc. Cary, NC, USA). A $p$ value of <0.05 was considered to indicate statistical significance.

## RESULTS

### Patient characteristics

Clinical background, blood biochemistry and virological data on CH (C) patients receiving peg-IFNα-2b plus ribavirin therapy are shown in Table 1. Eighty-six (86) of 151 patients (56.9%) were male, and 65 patients (43.1%) were female. The mean age was 54.9 years for males and 58.2 for females. Liver biopsy was performed in 81 (54%) of patients.

For the second group of patients (75), 45 (60%) were male and 30 (40%) patients were female. Liver biopsy was performed in 72 (47.7%) patients. Clinical background including age, male-female ratio, BMI, fibrosis staging, HCV RNA titers, Hgb and Plt values were not statistically different from those of first group of 151 patients (data not shown).

### Treatment efficacy and influencing factors

Seventy out of 151 patients (46.4%) achieved SVR (Table 2). The rate of EVR was 67%. The association between SVR rate and baseline clinical parameters before treatment or treatment-related factors was examined using univariate analysis.

**TABLE 1 Clinical Characteristics of Patients at Baseline (mean±SD)**

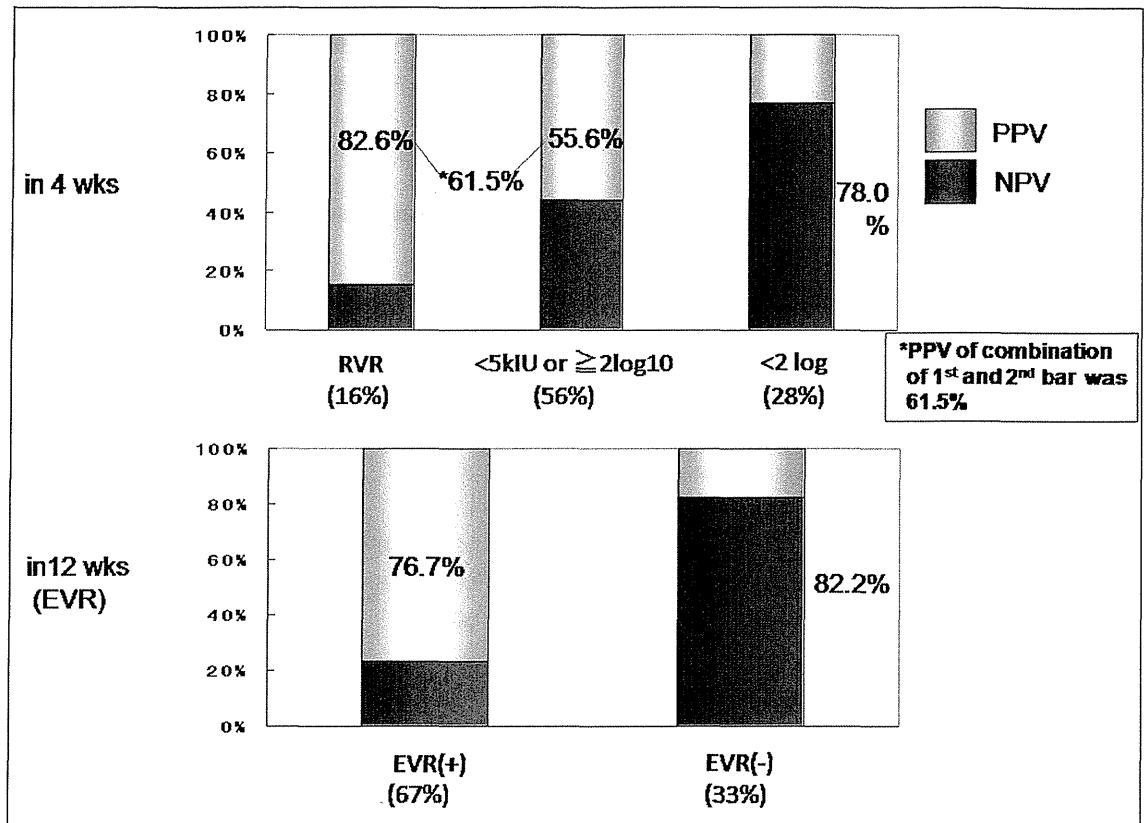| No. of Patients | 151 |
|---|---|
| Gender, n (%) | |
|   Male | 86 (56.9) |
|   Female | 65 (43.1) |
| Age (median, range, year) | |
|   M | 54.9±12.1 (21-74) |
|   F | 58.2±9.9 (21-71) |
| Body mass index | |
|   <25 | 103 (70.1) |
|   25≤ | 44 (29.9) |
| Histology | |
|   A 0-1/2-3 | 32/48 |
|   F 0-2/3-4 | 67/15 |
| HCV RNA titers ($\leq 10^3/10^3 <$ - $<10^4/10^4\leq$) (kIU/mL) | 27/94/30 |
| ALT (IU/L) (median, range) | 84.2±55.4 (70, 13-360) |
| Plt ($\times 10^4$/μL) | 15.8±5.4 (14.9, 5.9-35.8) |
| Hgb (g/dL) | 14.1±1.3 (14.1, 10.1-17.0) |

The following factors were analyzed: age, gender, BMI, previous interferon treatment, fibrosis, ALT, Plt, HCV RNA level, decrease in HCV RNA titers in the first 4 weeks of treatment, and level of adher-

**TABLE 2 Univariate Analysis of Association between Sustained Virological Response (SVR) and Influential Factors**

| Factors | SVR (n=70, 46.4%) | $p$ value |
|---|---|---|
| **Parameters before IFN treatment** | | |
| Age <60:≥60 | 40/82 (48.8%) : 30/69 (43.5%) | 0.6233 |
| Gender M : F | 41/86 (47.7%) : 29/65 (44.6%) | 0.7437 |
| BMI <25:≥25 | 49/103(47.6%) : 20/44 (45.4%) | 1.0 |
| **Previous interferon treatment** | | |
| (+) : (-) | 53/106 (50%) : 15/39 (38.5%) | 0.2617 |
| F0 -2 : 3-4 | 36/67 (53.7%) : 4/15 (47.4%) | 0.0860 |
| ALT (IU/L), <70 : ≥70 | 31/74 (41.9%) : 39/75 (52%) | 0.2519 |
| Plt (x$10^4$/mL), <15 : ≥15 | 23/70 (32.9%) : 38/68 (55.9%) | 0.0099* |
| **HCV RNA titers** | | |
| ≤103/103< - <104/104≤ | 15/27 (55.6%):43/94 (45.7%):12/30 (40.0%) | 0.2442 |
| **Decrease in HCV RNA in first 4 weeks** | | |
| Negative (RVR) : $\geq 2 \mathrm{Log}_{10}$ or <5kIU : $<2\mathrm{log}_{10}$ | 9/23(82.6%):45/81(55.6%):9/41(22.0%) | 0.0008* |
| **Peg-IFN 4 weeks adherence** | | |
| <80% : ≥80% | 7/20 (35.0%) : 62/129 (48.1%) | 0.3390 |
| **Peg-IFN 12 weeks adherence** | | |
| <80% : ≥80% | 7/27 (25.9%) : 62/122 (50.8%) | 0.0203* |
| **Ribavirin 12 weeks adherence** | | |
| <80% : ≥80% | 9/30 (30.0%) : 60/119 (50.4%) | 0.0643 |
| **Ribavirin 48 weeks adherence** | | |
| <80% : ≥80% | 29/85 (34.1%) : 36/60 (60.0%) | 0.0024* |

\*: statistically significant ($p<0.05$)

**FIGURE 1** Positive and negative predictive values for SVR with regard to the degree of viral decrease in the first 4 weeks (upper) and 12 weeks (lower) of therapy.



ence of peg-IFN and ribavirin. A summary of these results is shown in **Table 2**. The ratio of patients with Plt more than $15 \times 10^4/\mu L$, who achieved RVR or <5kIU/mL, more than $2\text{-log}_{10}$ decrease in the first 4 week, more than 80% adherence for 12 weeks peg-IFN and 80% adherence for 48 weeks ribavirin, were significantly higher in the SVR group than in the non-SVR group. The SVR rate in patients who achieved EVR was 76.7%, and this was significantly higher than the SVR rate in the non-EVR group which was 17.8% ($p<0.0001$, **Figure 1**, lower). For the factors determined to be as statistically significant on univariate analysis, we subsequently conducted multivariate analysis. Ribavirin adherence in the first 12 weeks, Plt counts and decreased HCV RNA in the first 4 weeks were independent predictive factors for SVR (**Table 3**).

For the evaluation of response-guided therapy, we focused on the relationship between viral decrease over for 4 weeks with therapy outcome. Positive and negative predictive values (PPV and NPV) for each degree of viral response at this time point for SVR are shown in **Figure 1**. PPV for patients with good viral response after 4 weeks (upper first two columns) was 61.5% and was lower when compared to 12-week EVR (76.7%). On the other hand, NPV for those who did not achieve a $2\text{-log}_{10}$ decrease in the first 4 weeks was high (78.0%), and was comparable to that for not achieving EVR after 12 weeks (82.2%). Thus not achieving a $2\text{-log}_{10}$ decrease after 4 weeks of therapy may be a good indicator for predicting non-SVR.

We examined core, NS5A (ISDR) substitution and CXCL10 values in 75 pretreatment serum samples from the second group of patients. Single core substitution, substitution number in ISDR, and CXCL10 levels were not found to be correlated with the endpoint (non-achievement of $2\text{-log}_{10}$ virus decrease after 4 weeks) (**Table 4**). Only patients with double core substitutions were significantly resistant to peg-IFNα-2b plus ribavirin therapy. However the number of patients who had this pattern of substitutions was very low (5/75, 6.7%)

## DISCUSSION

Early measurement of the virus during interferon-based treatment has been shown to be useful in determining the likelihood of response. Optimizing therapy duration based on the degree of virus decrease is called "response-guided therapy" and currently considered to be the most precise method for predicting the final outcome of therapy (17-22). Accurately predicting non-achievement of SVR can reduce unnecessary adverse effects and medical costs (17-22). On the other hand, patients can be motivated to adhere to therapy if high positive predictions of SVR can be made. Moreover, such predictors will allow the opportunity to reassess treatment plans. The primary aim of therapy may thus change from virus eradication to normalization of ALT values in order to slow down disease progression, and to suppress the incidence of HCC (24).

Viral decrease after 12 weeks of peg-IFNα-2b plus ribavirin may predict SVR after 48 weeks of

**TABLE 3** Multivariate Analysis of Association between Sustained Virological Response (SVR) and Influential Factors

| Factor | | Odds ratio | 95% confidential interval | p value |
|---|---|---|---|---|
| Ribavirin 12 weeks adherence | | | | |
| | <80% | 1 | | |
| | ≥80% | 4.279 | 1.157-15.821 | 0.0293* |
| Plt | <15x10$^4$ | 1 | | |
| | 15x10$^4$ | 2.716 | 1.004-7.352 | 0.0492* |
| HCV decrease at 4 week | | | | |
| | <2log$_{10}$ | 1 | | |
| | <5kIU or ≥2log$_{10}$ | 3.784 | 1.155-12.392 | 0.0279* |
| | negative | 7.342 | 1.558-34.610 | 0.0117* |

**TABLE 4** Univariate Analysis of Association between 2-log$_{10}$ decrease in HCV RNA in Initial 4 Weeks and Influential Factors

| Factors | | <2 log (n=20) : Others (n=55) | p value |
|---|---|---|---|
| Mutation at core | 70(+/-) | 7/20 (35.0%) : 15/55 (27.3%) | 0.572 |
| | 91 (+/-) | 8/19 (42.1%) : 14/56 (25.0%) | 0.242 |
| | Single mutant (either at 70 or 91) | 11/34 (32.4%) : 11/41 (26.8%) | 0.620 |
| | Double mutant (both at 70 or 91) | 4/5 (80%) : 18/70 (25.8%) | 0.024* |
| ISDR (Wild/Intermediate/Mutant) | | 8/10/3 : 20/21/6 | 0.809 |
| Serum IP-10 (pg/mL) | | 466.8±1488 : 517.8 ±325 | 0.634 |

treatment in patients with genotype 1b and high viral load patients. Negative HCV RNA (EVR) or at least a 2-log$_{10}$ decrease at this point is a necessary condition for SVR, the PPV of which has been reported to be about 70% (17). Patients who fail to achieve EVR would not clear the virus even after an additional 9 months therapy. In the present study, we particularly focused on the viral decrease during the first 4 weeks of therapy. This is because detection of virus RNA is covered by medical insurance only once per month in Japan, and most patients receive their first information on viral decreases at this hospital visit. They are typically eager to learn how the therapy is progressing and would like to receive some information regarding (dis)continuation of therapy. Based on the relatively high PPVs at this point, we showed that the achievement of negative or <5kIU/mL HCV RNA, or more than 2-log$_{10}$ decrease in the virus after 4 weeks of therapy still can be an important indicator for subsequent therapeutic planning, although these data are not as informative as those at 12 weeks (61.5% vs. 76.7%, **Figure** 1). Patients can receive encouragements to continue the therapy when they achieve this hurdle. Importantly, however, there is a high NPV at this point (78.0%), indicating that, with regard to the negative prediction of SVR, viral decrease in the first 4 weeks is as useful as EVR at 12 weeks (82.2%). Our pre-

liminary observations show that 8/14 (57%) of patients with a 1- to 2-log$_{10}$ decrease during 4 weeks achieved LVR (late viral response, HCV RNA became negative during 16 to 24 wks), and therefore might require 72 weeks of treatment (25). This response-guided concept after 4 weeks of treatment is beneficial, as it provides a preliminary chance to consider treatment outcome until the results of 12 weeks EVR are obtained.

We then examined the possible associations between virological factors including core and ISDR amino acid substitutions, as well as serum CXCL10 levels and <2log$_{10}$ decrease during the first 4 weeks of therapy, which is a good marker for non-SVR. Only double amino acid core substitutions seemed to be correlated with small viral decreases (**Table** 4). Although patient numbers with both substitutions were low in the present study (6.7%), our data provide some information on the negative prediction of viral response. A host genetic factor that affects virus response was recently identified (16) and genetic approaches may therefore provide valuable information in the future.

In conclusion, assessment of viral decrease after 4 weeks treatment with peg-IFNα-2b plus ribavirin is important in predicting therapy outcome, especially for non-response in the case of <2-log$_{10}$ decrease. Analysis of amino acids in the core region might confer useful information in some patients.

## REFERENCES

1. **Hayashi N, Takehara T:** Antiviral therapy for chronic hepatitis C: past, present, and future. J Gastroenterol 2006; 41:17-27.
2. **Zeuzem S:** Interferon-based therapy for chronic hepatitis C: current and future perspectives. Nat Clin Pract Gastroenterol Hepatol 2008; 5:610-22.
3. **Heathcote EJ:** Antiviral therapy: chronic hepatitis C. J Viral Hepat 2007; Suppl 1:82-8.
4. **Sroczynski G, Esteban E, Conrads-Frank A, et al:** Long-term effectiveness and cost-effectiveness of antiviral treatment in hepatitis C. J Viral Hepat 2010; 17:34-50.
5. **Manns MP, Wedemeyer H, Cornberg M:** Treating viral hepatitis C: efficacy, side effects, and complications. Gut 2006; 55:1350-9.
6. **Shiffman ML:** Side effects of medical therapy for chronic hepatitis C. Ann Hepatol 2004; 3:5-10.
7. **Maekawa S, Enomoto N:** Viral factors influencing the response to the combination therapy of peginterferon plus ribavirinavirin in chronic hepatitis C. J Gastroenterol 2009; 44:1009-15.
8. **Shirakawa H, Matsumoto A, Joshita S, et al:** Pretreatment prediction of virological response to peginterferon plus ribavirinavirin therapy in chronic hepatitis C patients using viral and host factors. Hepatology 2008; 48:1753-60.
9. **Okanoue T, Itoh Y, Hashimoto H, et al:** Predictive values of amino acid sequences of the core and NS5A regions in antiviral therapy for hepatitis C: a Japanese multicenter study. J Gastroenterol 2009; 44:952-63.
10. **Enomoto N, Sakuma I, Asahina Y, et al:** Mutations in the nonstructural protein 5A gene and response to interferon in patients with chronic hepatitis C virus 1b infection. N Engl J Med 1996; 334:77-81.
11. **Watanabe H, Enomoto N, Nagayama K, et al:** Number and position of mutations in the interferon (IFN) ensitivity-determining region of the gene for nonstructural protein 5A correlate with IFN efficacy in hepatitis C virus genotype 1b infection. J Infect Dis 2001; 183:1195-203.
12. **Akuta N, Suzuki F, Sezaki H, et al:** Association of amino acid substitution pattern in core protein of hepatitis C virus genotype 1b high viral load and non-virological response to interferon-ribavirinavirin combination therapy. Intervirology 2005; 48:372-80.
13. **Akuta N, Suzuki F, Kawamura Y, et al:** Predictive factors of early and sustained responses to peginterferon plus ribavirinavirin combination therapy in Japanese patients infected with hepatitis C virus genotype 1b: amino acid substitutions in the core region and low-density lipoprotein cholesterol levels. J Hepatol 2007; 46:403-10.
14. **Lagging M, Romero AI, Westin J, et al:** IP-10 predicts viral response and therapeutic outcome in difficult-to-treat patients with HCV genotype 1 infection. Hepatology 2006; 44:1617-25.
15. **Diago M, Castellano G, García-Samaniego J, et al:** Association of pretreatment serum interferon gamma inducible protein 10 levels with sustained virological response to peginterferon plus ribavirinavirin therapy in genotype 1 infected patients with chronic hepatitis C. Gut 2006; 55:374-9.
16. **Tanaka Y, Nishida N, Sugiyama M, et al:** Genome-wide association of IL28B with response to pegylated interferon-alpha and ribavirin therapy for chronic hepatitis C. Nat Genet 2009; 41:1105-9.
17. **Davis GL, Wong JB, McHutchison JG, Manns MP, Harvey J, Albrecht J:** Early virologic response to treatment with peginterferon alfa-2b plus ribavirinavirin in patients with chronic hepatitis C. Hepatology 2003; 38:645-52.
18. **Ferenci P:** Predicting the therapeutic response in patients with chronic hepatitis C: the role of viral kinetic studies. J Antimicrob Chemother 2004; 53:15-8.
19. **Zeuzem S, Berg T, Moeller B, et al:** Expert opinion on the treatment of patients with chronic hepatitis C. J Viral Hepat 2009; 16:75-90.
20. **Chevaliez S, Pawlotsky JM:** Practical use of hepatitis C virus kinetics monitoring in the treatment of chronic hepatitis C. J Viral Hepat 2007; 14Suppl1:77-81.
21. **Ferenci P, Laferl H, Scherzer TM, et al:** Peginterferon alfa-2a and ribavirin for 24 weeks in hepatitis C type 1 and 4 patients with rapid virological response. Gastroenterology 2008; 135:451-8.
22. **Lee SS, Ferenci P:** Optimizing outcomes in patients with hepatitis C virus genotype 1 or 4. Antivir Ther 2008; 13 Suppl 1:9-16.
23. **El-Shamy A, Nagano-Fujii M, Sasase N, et al:** Sequence variation in hepatitis C virus nonstructural protein 5A predicts clinical outcome of pegylated interferon/ribavirin combination therapy. Hepatology 2008; 48:38-47.
24. **Arase Y, Ikeda K, Suzuki F, et al:** Prolonged-interferon therapy reduces hepatocarcinogenesis in aged-patients with chronic hepatitis C. J Med Virol 2007; 79:1095-102.
25. **Watanabe S, Enomoto N, Koike K, et al:** Prolonged treatment with pegylated interferon alpha 2b plus ribavirin improves sustained virological response in chronic hepatitis C genotype 1 patients with late response in a clinical real-life setting in Japan. Hepatol Res 2010; 40:135-44.

9 Schick V, Franzius C, Beyna T et al. Diagnostic impact of 18F-FDG PET–CT evaluating solid pancreatic lesions versus endosonography, endoscopic retrograde cholangio-pancreatography with intraductal ultrasonography and abdominal ultrasound. Eur. J. Nucl. Med. Mol. Imaging 2008; 35: 1775–85.

10 Strobel K, Heinrich S, Bhure U et al. Contrast-enhanced 18F-FDG PET/CT: 1-stop-shop imaging for assessing the resectability of pancreatic cancer. J. Nucl. Med. 2008; 49: 1408–13.

11 Buchs NC, Bühler L, Bucher P et al. Value of contrast-enhanced 18F-fluorodeoxyglucose positron emission tomography/computed tomography in detection and presurgical assessment of pancreatic cancer: A prospective study. J. Gastroenterol. Hepatol. 2011; 26: 657–62.

# History and recent progress in evaluation of the fucosylated alpha-fetoprotein fraction

Yutaka Aoyagi, Yasushi Tamura and Takeshi Suda

Division of Gastroenterology and Hepatology, Department of Cellular Function, Course for Molecular and Cellular Medicine, Graduate School of Medical and Dental Sciences, Niigata University, Niigata, Japan

See article in J. Gastroenterol. Hepatol. 2011; 26: 739–744.

Hepatocellular carcinoma (HCC) is the fifth most common tumor and the third most common cause of cancer-related deaths worldwide.[1] Measurement of serum alpha-fetoprotein (AFP) concentration has been widely used for the detection of HCC during follow-up of patients with chronic liver disease, especially in hepatitis virus-related cirrhosis. However, the serum concentration of AFP also increases in non-neoplastic liver diseases such as hepatic cirrhosis and chronic hepatitis. Therefore, it is important to distinguish AFP species between HCC and non-neoplastic liver diseases.

Several investigators have reported that the measuring Lens culinaris agglutinin (LCA)-reactive fraction of AFP is useful for discrimination between the AFP species from HCC and from non-neoplastic liver diseases during follow-up of patients with chronic liver diseases.[2–4] That is, the percentage of LCA-reactive fraction of AFP in patients with HCC is significantly higher than in cases of non-neoplastic liver disease. More persuasive is a report of five HCC patients who showed a dramatic increase in LCA-reactive fraction of AFP in association with the development of HCC after a long history of hepatic cirrhosis.[5] This suggests that the levels of this fraction were a good measure for the onset of HCC.[6,7]

Since the above earlier reports, measurement of the fucosylated fraction of AFP has been used in clinical practice for early diagnosis of HCC, especially in Japan. Aoyagi and his colleague reported that three patients with cirrhosis for whom early recognition of HCC was made possible by the measurement of the fucosylated fraction of AFP. Increased levels of this fraction with a moderate increment of serum concentration of AFP were observed in three patients with cirrhosis who showed no indication of HCC by several imaging modalities. Four years after the onset of this increase in the fucosylated fraction, small HCC with a tumor diameter less than 2 cm was revealed in one case. In two other cases, small HCC were also detected 24 and 9 months, respectively, after the first sign of the increase in the fucosylated fraction. However, the development to HCC was not detected in five patients with cirrhosis in whom continuous increments of serum concentration of AFP with low levels of the fucosylated fraction were observed during the prospective follow-up from 3 to 9 years. These findings indicated that the fucosylated fraction of AFP can be used as an aid in an early recognition of HCC, especially in patients with cirrhosis during the follow-up process in which the moderate increment of serum concentration of AFP is noted.[8] Similar findings, that early recognition of HCC can be based on altered profiles of AFP, have been reported by Sato et al.[9]

The molecular basis of the LCA-reactive fraction of AFP is fucosylation of the biantennary sugar chain at the innermost N-acetylglucosamine residue.[10,11] It was formerly measured by lectin affinity electrophoresis in the presence of LCA, a method devised by Taketa and Hirai.[12] The lower limit for detection of serum AFP concentration is around 30 ng/mL, although it depends on the percentage of fucosylated fraction in total AFP. Accordingly, the fucosylated fraction of AFP was measured in patients with AFP concentrations more than this level for the early diagnosis of HCC. Since then, a sensitive measuring device for fucosylated fraction of AFP, liquid-phase binding assay; LiBASys (Wako Pure Chemical Industries Ltd. Osaka, Japan) has been developed, and the present lower limit of serum AFP is 10 ng/mL. More recently, a more sensitive automated immunoassay using on-chip electrokinetic reaction and separation by affinity electrophoresis (micro-total analysis system; μ-TAS, Wako Pure Chemical Industries Ltd) has been developed.[13,14] This highly sensitive system involves microchip capillary electrophoresis and a liquid-phase binding assay system. The assay can detect the fucosylated fraction in AFP concentrations that exceed 2 ng/mL.

In this issue of the Journal of Gastroenterology and Hepatology,[15] Hanaoka and his colleagues demonstrate the clinical significance of high sensitive fucosylated fraction of AFP (hs-AFP-L3) by a μ-TAS device in chronic liver diseases with very low serum AFP concentrations, that is, between 3 and 10 ng/mL. A total of 241 patients with chronic liver disease were enrolled; hs-AFP-L3 could be detectable in 60 patients. Among them, HCC became prevalent in 20 patients (33%) out of 60, while HCC was found in 16 patients (9% of 181 cases) without positivity of hs-AFP-L3. The superiority of hs-AFP-L3 is statistically significant. The cut-off value of hs-AFP-L3 was set at 5.75% by a receiver operating characteristic (ROC) curve. Furthermore, HCC was newly detected in six patients (22%) in the hs-AFP-L3 elevated group and in 10 (5.6%) in the non-elevated group during the follow-up period. Analysis using the Kaplan–Meier method showed the HCC-free rate of the hs-AFP-L3 elevated group was significantly

lower than that of the non-elevated group ($P = 0.0038$). Finally, hs-AFP-L3 was one of several independent predicting variants ($P = 0.0036$) for HCC development by multivariate analyses.

The data presented here are convincing and give valuable information for the early diagnosis of HCC during the follow-up of patients with chronic liver diseases. However, two concerns can be raised about interpretation of the present manuscript. First, the ROC curve (Fig. 2) in this study was slightly "bumpy," and the cut-off value, 5.75% obtained by the ROC curve may not be reliable. A cut-off value of 10% by the former assay system of LiBASys is generally accepted in Japan. Recently, Tamura *et al.* reported the clinical advantage of the same high sensitive immunoassay for fucosylated fraction of AFP.[16] Serum fucosylated fraction of AFP was measured in 295 patients with HCC and 350 with benign liver diseases. The diagnostic accuracy of the current μ-TAS AFP-L3 was compared with that of the former conventional assay device, LiBASys. When the cut-off value was set at 7%, the sensitivity, specificity, accuracy, positive predictive value and negative predictive value of μ-TAS AFP-L3 were 60%, 90% 76%, 84%, and 73%, respectively. Its sensitivity was particularly good (41%) in the HCC subgroups with lower AFP concentrations (< 20 ng/mL). The positivity rates for μ-TAS AFP-L3 were higher at each tumor stage than those of LiBASys AFP-L3 (μ-TAS/LiBASys: stage I, 44%/16%; stage II 53%/38%; stage III 66%/45%; stage IV 83%/66%). Thus, μ-TAS AFP-L3 appears to be more sensitive for discriminating HCC than the conventional LiBASys AFP-L3, particularly in subgroups with lower AFP concentrations and early-stage HCC.

The second concern is that the multivariate analysis of factors affecting future occurrence of HCC was investigated in this report by Cox's proportional-hazard model, and only two factors, female gender and hs-AFP-L3 were identified as significant. However, only six factors were enrolled in the analysis. Besides these factors, age, etiology of cirrhosis, presence or absence of diabetes mellitus, presence or absence of interferon treatment, nucleoside analogue treatment, obesity and severity of cirrhosis such as platelet count are essential.

In conclusion, the highly sensitive measurement of hs-AFP-L3 now appears to be a very useful and practical tool for the early diagnosis of HCC when the serum concentrations of AFP are less than 10 ng/mL, as shown by Hanaoka and colleagues in the present issue of JGH. To reconfirm the present results, however, a large scale prospective multicenter study will be required.

## References

1 Parkin DM, Bray F, Ferlay J *et al.* Estimating the world cancer burdenGLOBOCAN2000. *Int. J. Cancer* 2001; **94**: 153–6.

2 Breborowicz J, Mackiewicz A, Breborowicz D. Microheterogeneity of alpha-fetoprotein in patient serum as demonstrated by lectin affino-electrophoresis. *Scand. J. Immunol.* 1981; **14**: 15–20.

3 Aoyagi Y, Suzuki Y, Isemura M *et al.* Differential reactivity of alpha-fetoprotein with lectins and evaluation of its usefulness in the diagnosis of hepatocellular carcinoma. *Gann* 1984; **75**: 809–15.

4 Aoyagi Y, Isemura M, Suzuki Y *et al.* Fucosylated alpha-fetoprotein as marker of early hepatocellular carcinoma. *Lancet* 1985; **ii**: 1353–4.

5 Aoyagi Y, Isemura M, Suzuki Y *et al.* Change in fucosylation of alpha-fetoprotein on malignant transformation of liver cells. *Lancet* 1986; **I**: 210.

6 Aoyagi Y, Suzuki Y, Isemura M *et al.* The fucosylation index of alpha-fetoprotein and its usefulness in the early diagnosis of hepatocellular carcinoma. *Cancer* 1988; **61**: 769–74.

7 Taketa K, Sekiya C, Namiki M *et al.* Lectin-reactive profiles of alpha-fetoprotein characterizing hepatocellular carcinoma and related conditions. *Gastroenterology* 1990; **99**: 508–18.

8 Aoyagi Y, Saitoh A, Suzuki Y *et al.* Fucosylation index of alpha-fetoprotein, a possible aid in early recognition of hepatocellular carcinoma in patients with cirrhosis. *Hepatology* 1993; **17**: 50–2.

9 Sato Y, Nakata K, Kato Y *et al.* Early recognition of hepatocellular carcinoma based on altered profiles of alpha-fetoprotein. *N. Engl. J. Med.* 1993; **328**: 1802–6.

10 Aoyagi Y, Isemura M, Yosizawa Z *et al.* Fucosylation of serum alpha-fetoprotein in patients with primary hepatocellular carcinoma. *Biochim. Biophys. Acta* 1985; **830**: 217–23.

11 Aoyagi Y, Suzuki Y, Igarashi K *et al.* Carbohydrate structures of human alpha-fetoprotein of patients with hepatocellular carcinoma: presence of fucosylated and non-fucosylated triantennary glycans. *Br. J. Cancer* 1993; **67**: 486–92.

12 Taketa K, Hirai H. Lectin affinity electrophoresis of alpha-fetoprotein in cancer diagnosis. *Electrophoresis* 1989; **10**: 562–7.

13 Kagebayashi C, Yamaguchi I, Akinaga A *et al.* Automated immunoassay system for AFP-L3% using on-chip electrokinetic reaction and separation by affinity electrophoresis. *Anal. Biochem.* 2009; **388**: 306–11.

14 Kawabata T, Wada HG, Watanabe M, Satomura S. Electrokinetic analyte transport assay for alpha-fetoprotein immunoassay integrates mixing, reaction and separation on-chip. *Electrophoresis* 2008; **29**: 1399–406.

15 Hanaoka T, Sato S, Tobita H *et al.* Clinical significance of the highly sensitive fucosylated fraction of α-fetoprotein in patients with chronic liver disease. *J. Gastroenterol. Hepatol.* 2011; **26**: 739–44.

16 Tamura Y, Igarashi M, Kawai H, Suda T, Satomura S, Aoyagi Y. Clinical advantage of highly sensitive on-chip immunoassay for fucosylated fraction of alpha-fetoprotein in patients with hepatocellular carcinoma. *Dig. Dis. Sci.* 2010; **55**: 3576–83.

# New contrast enhanced ultrasonography agent: Impact of Sonazoid on radiofrequency ablation

Atsushi Hiraoka,*,† Yoichi Hiasa,† Morikazu Onji† and Kojiro Michitaka*,†

*Gastroenterology Center, Ehime Prefectural Central Hospital, Matsuyama, and †Department of Gastroenterology and Metabology, Ehime University Graduate School of Medicine, Ehime, Japan

See article in *J. Gastroenterol. Hepatol.* 2011; 26: 759–764.

**Correspondence**

Dr Atsushi Hiraoka, Ehime Prefectural Central Hospital, Kasuga-Cho 83, Matsuyama, Ehime 790-0024, Japan. Email: hirage@m.ehime-u.ac.jp

# The initial phase of chromosome condensation requires Cdk1-mediated phosphorylation of the CAP-D3 subunit of condensin II

Satoshi Abe,[1,2,6] Kota Nagasaka,[1,3,6] Youko Hirayama,[1] Hiroko Kozuka-Hata,[4] Masaaki Oyama,[4] Yutaka Aoyagi,[2] Chikashi Obuse,[5] and Toru Hirota[1,3,7]

[1]Cancer Institute, Japanese Foundation for Cancer Research (JFCR), Tokyo 135-8550, Japan; [2]Niigata University Graduate School of Medical and Dental Sciences, Niigata 951-8122, Japan; [3]Graduate School of Bioscience and Biotechnology, Tokyo Institute of Technology, Yokohama 226-8501, Japan; [4]Institute of Medical Science, University of Tokyo, Tokyo 108-8639, Japan; [5]Graduate School of Life Science, Hokkaido University, Sapporo 001-0021, Japan

The cell cycle transition from interphase into mitosis is best characterized by the appearance of condensed chromosomes that become microscopically visible as thread-like structures in nuclei. Biochemically, launching the mitotic program requires the activation of the mitotic cyclin-dependent kinase Cdk1 (cyclin-dependent kinase 1), but whether and how Cdk1 triggers chromosome assembly at mitotic entry are not well understood. Here we report that mitotic chromosome assembly in prophase depends on Cdk1-mediated phosphorylation of the condensin II complex. We identified Thr 1415 of the CAP-D3 subunit as a Cdk1 phosphorylation site, which proved crucial as it was required for the Polo kinase Plk1 (Polo-like kinase 1) to localize to chromosome axes through binding to CAP-D3 and thereby hyperphosphorylate the condensin II complex. Live-cell imaging analysis of cells carrying nonphosphorylatable CAP-D3 mutants in place of endogenous protein suggested that phosphorylation of Thr 1415 is required for timely chromosome condensation during prophase, and that the Plk1-mediated phosphorylation of condensin II facilitates its ability to assemble chromosomes properly. These observations provide an explanation for how Cdk1 induces chromosome assembly in cells entering mitosis, and underscore the significance of the cooperative action of Plk1 with Cdk1.

Cells pass their genome from one to the next by forming mitotic chromosomes that become discernible as cells divide. Such large-scale reorganization of chromatin fibers into mitotic chromosomes depends on chromosome condensation and dissociation of sister chromatid cohesion. These two processes, together constituting mitotic chromosome assembly, initiate in prophase and are thought to ensure the correct orientation of chromosomes on the mitotic spindle and the faithful separation of sister chromatids in anaphase. The mitotic cyclin-dependent kinase 1 (Cdk1) has a fundamental function to drive cells into mitosis, as cells, in principle, do not initiate the mitotic entry program in the absence of Cdk1 activity (Nurse 1990; Nigg 1995). Despite its undisputed role in inducing the mitotic program, surprisingly few

substrates for Cdk1 have been identified to date. Thus, finding direct substrates for Cdk1 in this context continues to be a major challenge in order to elucidate the molecular mechanisms underlying morphological changes as cells enter mitosis, including chromosome assembly.

Mitotic chromosome assembly is mediated primarily through the activity of Smc (structural maintenance of chromosomes) protein complexes called condensins (for review, see Hirano 2005; Nasmyth and Haering 2005). Two classes of condensin complex, termed condensin I and II, have been identified in metazoans that share the core two ATPases—Smc2 and Smc 4 (also known as CAP-E and CAP-C, respectively)—and contain different, yet related, sets of non-Smc subunits. In human cells, non-Smc subunits of condensin I include CAP-D2, CAP-G, and CAP-H (also known as Kleisin-γ), and the respective counterparts in the condensin II complex are called CAP-D3, CAP-G2, and CAP-H2 (also known as Kleisin-β) (Ono et al. 2003; Yeong et al. 2003). Despite these structural similarities, condensin I and condensin II behave differently

- 367 -

from each other and have distinct functions during mitotic chromosome assembly (Hirota et al. 2004; Ono et al. 2004). Condensin I localizes in the cytoplasm until the nuclear envelope breakdown (NEBD), and gains access to chromosomes thereafter to confer physical properties to chromosomes required to withstand spindle-pulling forces (Gerlich et al. 2006). Condensin II, in contrast, localizes in the nucleus and thus can accumulate at chromosome axes from early stages of prophase. Consistent with this observation, the activity of condensin II is indispensable to initiate chromosome condensation in prophase (Hirota et al. 2004; Ono et al. 2004).

The activity of condensin is stimulated during mitosis when condensin subunits are phosphorylated (for review, see Hirano 2009). Seminal experiments using frog egg extracts showed that the activity of condensin, quantified by measuring its ability to induce supercoils into DNA substrates, is stimulated during mitosis when condensin I subunits are phosphorylated by Cdk1 (Kimura et al. 1998). The requirement of another major mitotic kinase, Aurora B, for the association of condensin I to chromosomes is widespread in metazoans (Giet and Glover 2001; Hagstrom et al. 2002; Kaitna et al. 2002; Petersen and Hagan 2003; Lipp et al. 2007; Takemoto et al. 2007). Similarly, in budding yeast, whose single class of condensin is structurally related to vertebrate condensin I, condensin is phosphorylated by the Aurora kinase Ipl1 (Lavoie et al. 2004). Moreover, in this organism, the Polo kinase Cdc5 has been found recently to phosphorylate condensin and promote supercoiling activity and chromosome condensation in anaphase (St-Pierre et al. 2009). In contrast to what had been unraveled for condensin I regulation, it is largely unknown how condensin II is controlled, however.

What are the mechanisms that drive condensation of the duplicated chromosomes as the cell enters mitosis? Because condensin II is the only chromosomal component that is known to be essential for timely chromosome condensation in prophase (Hirota et al. 2004; Ono et al. 2004), elucidating the regulation of condensin II would provide a clue to this long-standing question. Here we described that chromosome condensation in prophase depends on Cdk1-mediated phosphorylation of the CAP-D3 subunit of condensin II. We found that Cdk1 phosphorylation of the Thr 1415 residue allows Plk1 (Polo-like kinase 1) recruitment to CAP-D3 and the chromosomal axis, which then propagates phosphorylation of the whole condensin II complex. Replacement of endogenous CAP-D3 by nonphosphorylatable mutants indicated that the phosphorylation of Thr 1415 triggers chromosome condensation in prophase and stimulates condensin II-mediated assembly of chromosomes. Defining CAP-D3 as a physiological substrate of Cdk1 provides a molecular explanation for how Cdk1 triggers mitotic chromosome assembly.

## Results

### Plk1 binds to the condensin II complex

To address how condensin II is regulated in mitosis, we searched for proteins that bind to condensin II in mitotic

cell extracts. Mass spectrometric analysis of immunoprecipitates using antibodies to the condensin II subunit CAP-D3 identified the Polo kinase Plk1 as a candidate binding protein of condensin II. To validate this interaction, we performed an immunoprecipitation assay using different polyclonal antibodies to condensin II subunits. All of the antibodies used immunoprecipitated Plk1 as well as condensin II components from mitotic cell extracts (Supplemental Fig. 1A). Coimmunoprecipitation of Plk1 was seen more clearly when condensin II complexes were purified from a mitotic chromosome-enriched fraction, implying that the interaction occurs predominantly on chromosomes (Fig. 1A).

One mode of interaction of Plk1 with its binding proteins is via a phospho-Ser/Thr-binding motif called the polo-box domain (PBD) (Elia et al. 2003). To address whether Plk1 binds directly to condensin II—and, if so, which of the condensin subunits binds to Plk1—the condensin II complex purified from mitotic cell extracts was subjected to Far-Western analysis using recombinant PBD protein as a probe. We found a PBD signal on the CAP-D3 protein but not on the other subunits (Fig. 1B). The signal appeared to react specifically to a phosphorylated form of CAP-D3, which was revealed by retarded electrophoretic mobility in a polyacrylamide gel (Yeong et al. 2003; Lipp et al. 2007). Supporting this idea, this binding of PBD was diminished when isolated condensin II was pretreated with protein phosphatase (Fig. 1B). These data suggested that Plk1 binds directly to CAP-D3 in a phosphorylation-dependent manner.

### Mitotic phosphorylation of condensin II depends on both Cdk1 and Plk1

It has been shown that non-Smc subunits of condensin are phosphorylated in mitosis, some of which can be indicated by their electromobility shifts (Fig. 1C; Yeong et al. 2003). To be able to detect phosphorylated species more clearly, we used a Phos-tag acrylamide gel mixture for SDS-PAGE, which allowed us to differentiate the mobility shifts for all condensin non-Smc subunits (Fig. 1D). We then addressed which of the mitotic kinases are involved in the phosphorylation of condensin II. We found that a 20-min pretreatment of mitotic cells with a Cdk1 inhibitor abolished the mitotic mobility retardation of both condensin I and condensin II subunits. Plk1 inhibition largely reversed the mobility shifts for condensin II subunits. Among them, the mitotic retardation of CAP-D3 was markedly suppressed by Plk1 inhibition, implying that hyperphosphorylation of this protein depends on Plk1 activity, but some shift-up still remained, which appeared to depend on Cdk1 activity (Supplemental Fig. 1B). In contrast, Plk1 inhibition did not detectably affect the mitotic mobility retardation for condensin I subunits (Fig. 1D). These experiments suggested that mitotic phosphorylation of condensin II depends on both Cdk1 and Plk1. Consistent with this idea, a large-scale proteomic analysis has recently found condensin II subunits as Plk1 substrates (Santamaria et al. 2011).

To investigate how these kinases are involved in regulating condensin II, we first generated cell lines that
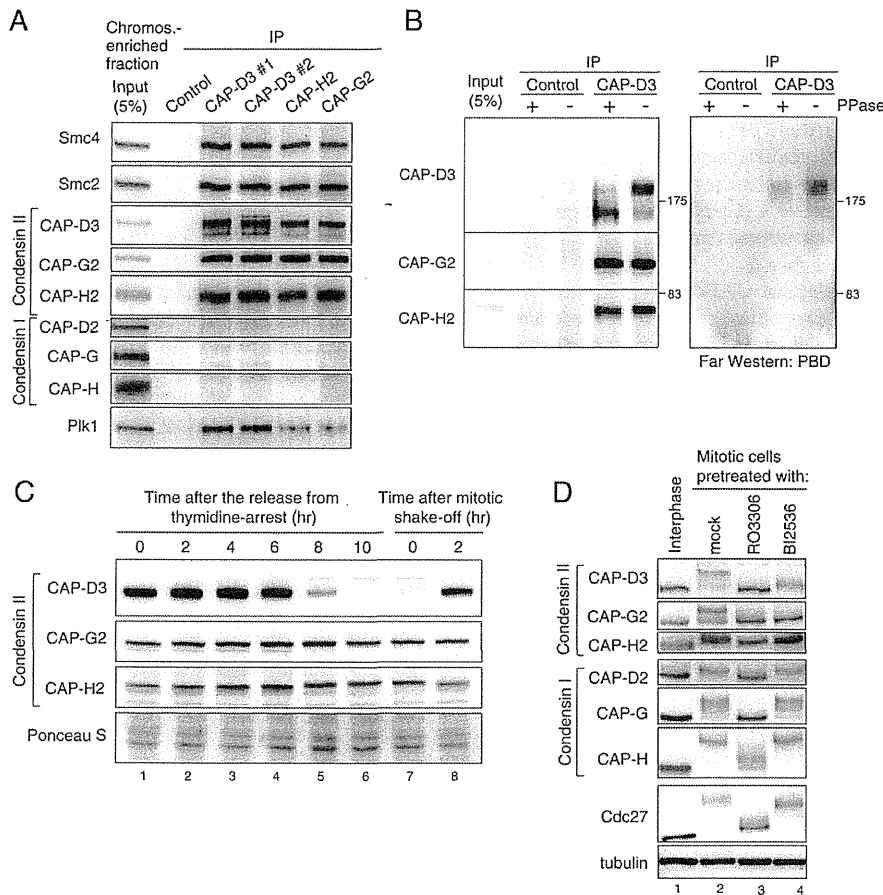
**Figure 1.** Regulation of condensin II in mitosis. (A) Immunoprecipitation of Plk1 with condensin II. Condensin II components were immunoprecipitated from a chromosome-enriched fraction prepared from mitotic cell extracts using either of two different antibodies to CAP-D3 (#1 or #2), CAP-G2, CAP-H2, or nonimmune IgG as a control, and resulting precipitates (IP) were analyzed by immunoblotting with the antibodies indicated. Note that none of the condensin I subunits copurified with the condensin II complex, discounting the possibility that the interaction between condensin II and Plk1 is mediated indirectly by DNA. (B) Plk1 binds directly to CAP-D3 in a phosphorylation-dependent manner. Immunoprecipitates with either control or CAP-D3 antibodies from mitotic cell extracts were incubated with or without phosphatase (PPase), and were analyzed by immunoblotting with indicated antibodies (left panel) and Far-Western blotting with PBD (right panel). (C) Detection of CAP-D3 phosphorylation in mitotic cell extracts. Synchronized cell populations were analyzed by immunoblotting at the indicated times after the release from thymidine arrest (i.e., early S phase) (lanes 1–6) or nocodazole arrest (i.e., mitosis) (lanes 7,8). As reported previously (Yeong et al. 2003; Lipp et al. 2007), slowly migrating bands of CAP-D3 were detected specifically during mitosis, but little retardation was detectable for CAP-G2 and CAP-H2. (D) Mitotic phosphorylation of condensin II depends on Cdk1 and Plk1. Thymidine-arrested interphase cells (lane 1), nocodazole-arrested mitotic cells (lane 2), a Cdk1 inhibitor RO3306-treated nocodazole-arrested mitotic cell (lane 3), or a Plk1 inhibitor BI2536-treated nocodazole-arrested mitotic cell (lane 4) were analyzed by immunoblotting for condensin subunits. The mobility shifts for Cdc27 verify that these pretreatments efficiently abolished the activities of the targeted kinases in mitotic cells (Kraft et al. 2003).

express GFP-tagged CAP-D3 at physiological levels, which appeared to possess tested properties of the endogenous protein (Supplemental Fig. 2A–C). We could also show that the GFP-tagged protein is functional, as the cell line expressing GFP-CAP-D3 showed a rescue of phenotypic defects observed after suppression of the endogenous gene by RNAi in analyses below. The finding that the association of Plk1 with CAP-D3 requires phosphorylation of CAP-D3 led us to predict that CAP-D3 contains the PBD-binding motif S-pS/pT-P (Elia et al. 2003). To obtain an objective picture of CAP-D3 phosphorylation,

we performed mass spectrometric analysis of immuno-purified CAP-D3 from mitotic cells (Supplemental Fig. 3). Among the phosphorylated residues suggested, Ser 1329 and Thr 1415 were found to meet the consensus of the PBD-binding motif.

In human CAP-D3, there are three sites in total that meet the PBD-binding motif, including the above two. To address whether any of these candidate sites are involved in the interaction with Plk1, we generated cell lines that express a series of GFP-tagged nonphosphorylatable mutants of full-length CAP-D3 by changing one of the